

SEDIMENT FLUX THROUGH THE RIO GRANDE RIVER:

A MONSOONAL EFFECT

Troy C.Hiatt

A thesis submitted to the faculty of
Brigham Young University
in partial fulfillment of the requirements for the degree of

Master of Science

Summer Rupper
Thomas Morris
John McBride

Department of Geological Sciences

Brigham Young University

August 2010

Copyright © 2010 Troy C. Hiatt

All Rights Reserved

ABSTRACT

Sediment Flux through the Rio Grande River: A Monsoonal Effect

Troy C. Hiatt

Department of Geological Sciences

Master of Science

Climate has historically been recognized as an influence on sediment flux and deposition. The North American Monsoon is suggested as the forcing mechanism of deltaic progradational events of the Rio Grande River delta. Interpretations of reflection seismic profiles reveal that eustatic rise in sea-level from the Last Glacial Maximum to present is accompanied by several regressional events of the Rio Grande delta 5.5, 9.5, and 11.5 ka BP. Much of the migration of depositional facies within a delta system is forced by hinterland tectonics and base-level rise and fall. However, we suggest that the movement of facies within the Rio Grande delta system represent climate forcing as the most dominant influence on sediment deposition during this short time period. While dominance of climate influence is possible, the sensitivity of an increase in monsoon precipitation and its effect on sediment flux has not yet been tested. We test monsoonal effects using relationships between sediment flux, river discharge, and precipitation. Heavy water management and withdrawal and complexity of precipitation timing and events within the region make the relationship between precipitation and sediment flux difficult to quantify using modern data sources. Therefore, it is necessary to numerically simulate stream discharge to test potential sensitivities of the system to monsoonal precipitation using a stream discharge model. Precipitation input into the stream discharge model is gathered from a suite of climate model simulation outputs. Suspended sediment flux is derived from the outputs of the flow models using empirically derived sediment rating curves. Results of sediment modeling show that increased precipitation during the monsoon months of July-September, 6 ka BP increased monthly suspended sediment flux by 79 percent. The suite of climate models does not include 9 or 11 ka BP, but we suggest the monsoon may have been stronger during this time based on greater received insolation at these times. This study also shows that duration and intensity of monsoonal precipitation events can more greatly affect stream discharge and sediment flux than increased precipitation with constant storm intensity.

ACKNOWLEDGEMENTS

First of all, I'd like to thank my advisor, Summer, for all the patience she exercised in training me to become a scientist. Summer has one of those powerful, analytical minds that not everyone is fortunate enough to have, and she shared a little bit of her know-how with me. Thanks to her, I have received on-the-job scientist training. My deepest gratitude goes out to her for tirelessly explaining redundant information to me until I could comprehend the subject matter.

I'd also like to thank Tom Morris and John McBride. My gratitude to Tom for his cool, level-headed advice regarding matters related or not related to my thesis. Academic wisdom is paramount as a professor, but the thoughts and experiences shared over and above academia are invaluable to me as a person. Thanks to John for his professional opinions regarding not just the thesis itself, but a bigger picture of applicability and practicality within the scientific community; all done with smartly timed comedy.

Jim Nelson of the civil engineering department is especially deserving of my gratitude. I undertook the ArcGIS for civil engineers class fall of 2009. Feared by many of my colleagues before me, the class was as much enjoyable as it was challenging. Jim offered his time and expertise during several meetings throughout the course of the semester. He also allotted me several complimentary copies of WMS 8.2, a costly program.

Lastly I'd like to thank all of those supporting roles: Nathaniel Jones for his tireless explanations and help with Matlab; Annika Quick for her geospatial assistance; and my friends and family for their dependability.

Table of Contents

List of Tables	vii
List of Figures	viii
INTRODUCTION	1
BACKGROUND	2
The North American Monsoon	2
Rio Grande setting and history	5
Rio Grande delta	6
Objective	8
METHODS	9
Stream discharge-sediment relationship	9
Precipitation-stream discharge relationship	11
Watershed modeling	13
Determination of watershed curve number	14
Regional climate proxy data	18
General Circulation Models	20
Boundary conditions	21
Insolation	22
GCM data	24
GCM results	26
GCM results and paleoclimate proxy data	31
Storm frequency and concentration	32
Frequent storms vs. constant precipitation	32
Regional storm concentration	33
Sediment simulation	36
DISCUSSION	40
Monsoon strength and impacts on sediment through time	40
Sediment Simulation Method	41
The Younger Dryas	42
Model simplicity and bedload	42
Future work	43
CONCLUSION	44
REFERENCES	46

List of Tables

1. Curve numbers, as defined by land-use codes and soil types
2. Input boundary conditions for PMIP 0 ka, 6 ka, and 21 ka climate simulation models
3. Insolation values for 30°N from the last glacial maximum to present
4. Average days per storm and average storms per month
5. Sediment experiment runs with precipitation input, raw sediment values, net difference, and percent difference

List of Figures

1. Index map of regional highlands and surrounding water
2. Rio Grande watershed and regional annual summer monsoon precipitation
3. Interpreted profile of the upper-most units of the Rio Grande delta in the Gulf of Mexico
4. Location of the southernmost stream gauge, 08358300
5. Major dams within and around the New Mexico-Colorado portion of the Rio Grande watershed
6. Distribution of curve numbers throughout the New Mexico and Colorado portion of the Rio Grande watershed
7. Locations of regional paleoclimate studies
8. Index of climate wetness according to regional paleoclimate studies
9. Insolation from the sun during June at 30°N on the earth's surface
10. Locations of extracted grid cells for the MIRO model run
11. 0 ka GCM precipitation simulation for the upper cell block with monthly model standard deviation attached to the average trend line
12. Temperature Anomaly for 6 ka model runs
13. Average monthly precipitation anomaly for 6 ka
14. Comparisons of multi-event, 10-day storm versus constant 10 day precipitation
15. Locations of the rain gauges for the longest running precipitation records within the state of New Mexico
16. The Type-II 24 hour curve as defined in the WMS software
17. Plot of 6 ka-0 ka simulated suspended sediment flux and the percent difference based on the three experiments: 4, 2, and 6 storms/ month

INTRODUCTION

Basinal base-level fluctuation and hinterland tectonics significantly influence fluvial sediment flux and deltaic depositional potential (Wellner and Bartek, 2003; Van Wagoner et al., 1990; Blum and Tornqvist, 2000). Climatic influence has also been recognized as a forcing mechanism on sediment transport and deposition (Blum and Tornqvist, 2000; others). However, climate is not physically recorded in the rock record like base-level change or hinterland tectonics and, therefore, its influence on the rock record is less understood by geologists. It is well understood that climatologically forced increases in precipitation could cause increased stream discharge and flow velocity, which, in turn, could cause increased sediment flux in a stream. Therefore, testing the sensitivity of fluvially transported sediment to changes in climate for a given watershed is in order (Zhua et al., 2008; Syvitski and Andrews, 1994).

Present-day monsoon influence and potentially larger influence in the past, along with anomalous depositional features in the Rio Grande delta, prompt use of the Rio Grande River to test the sensitivity of sediment transport to change in climate. The Rio Grande River delta system in the Gulf of Mexico (GOM) contains lobes that were prograding over the shelf edge during eustatic transgression (Banfield, 2008). This transgression began 17 ka B. P. (Curry, 1959). Climate, in particular, monsoonal variations, was proposed by Wellner et al. (2000) and Banfield and Anderson (2004) to explain these anomalous fluxes in sediment deposition. Though a sensitivity test of sediment flux to increased precipitation does not fully explain the mechanism or quantity of sediment seen in the Rio Grande River delta, it provides understanding that climate can reasonably influence sediment flux out of the system. We herein examine the sensitivity of sediment flux to changes in the North American Monsoon (NAM) within the Rio

Grande watershed using empirically derived sediment-water flux relationships, general circulation model output, and watershed modeling. This study differs from previous sensitivity tests (Zhua et al., 2008; Syvitski and Andrews, 1994) in that it:

1. studies a new location
2. uses paleoclimate model output data as input
3. and tests the sensitivity of change in model boundary conditions on sediment flux.

BACKGROUND

The North American Monsoon

The NAM is centered in north-central Mexico and influences several southwestern states of the U.S. This monsoon region is bounded by cool Pacific water directly to the west and warm ocean water in the Gulf of California, southward in the Pacific Ocean, and the GOM. Prevalent highlands in the region include the Colorado Plateau, Basin and Range, Sierra Madre Occidental, Mexican Altiplano, and the Sierra Madre Oriental (Figure 1). Seasonal warming of the continent coupled with copious moisture sourced from neighboring bodies of water creates an area conducive to monsoons (Adams and Comrie, 1997).

By definition, the monsoon is a seasonal shift in the prevailing winds. The shift is caused by northward expansion of the Azores High, a semi-permanent high pressure region located in the Atlantic Ocean. This intrusion of high pressure causes the dry southwest wind to be replaced by a humid southeast wind. This finding sparked large debate concerning where the moisture comes from (Reitan, 1957; Rasmusson, 1976; Bryson and Lowry, 1955), but presently most researchers agree that low-level moisture comes from the eastern tropical-Pacific and Gulf of California, and high-level moisture comes from the GOM (Harrington et al, 1992, Watson et al,

1994, Schmitz and Mullen, 1996). These moisture sources are mixed over the Sierra Madre Occidental before being transported into the U.S.

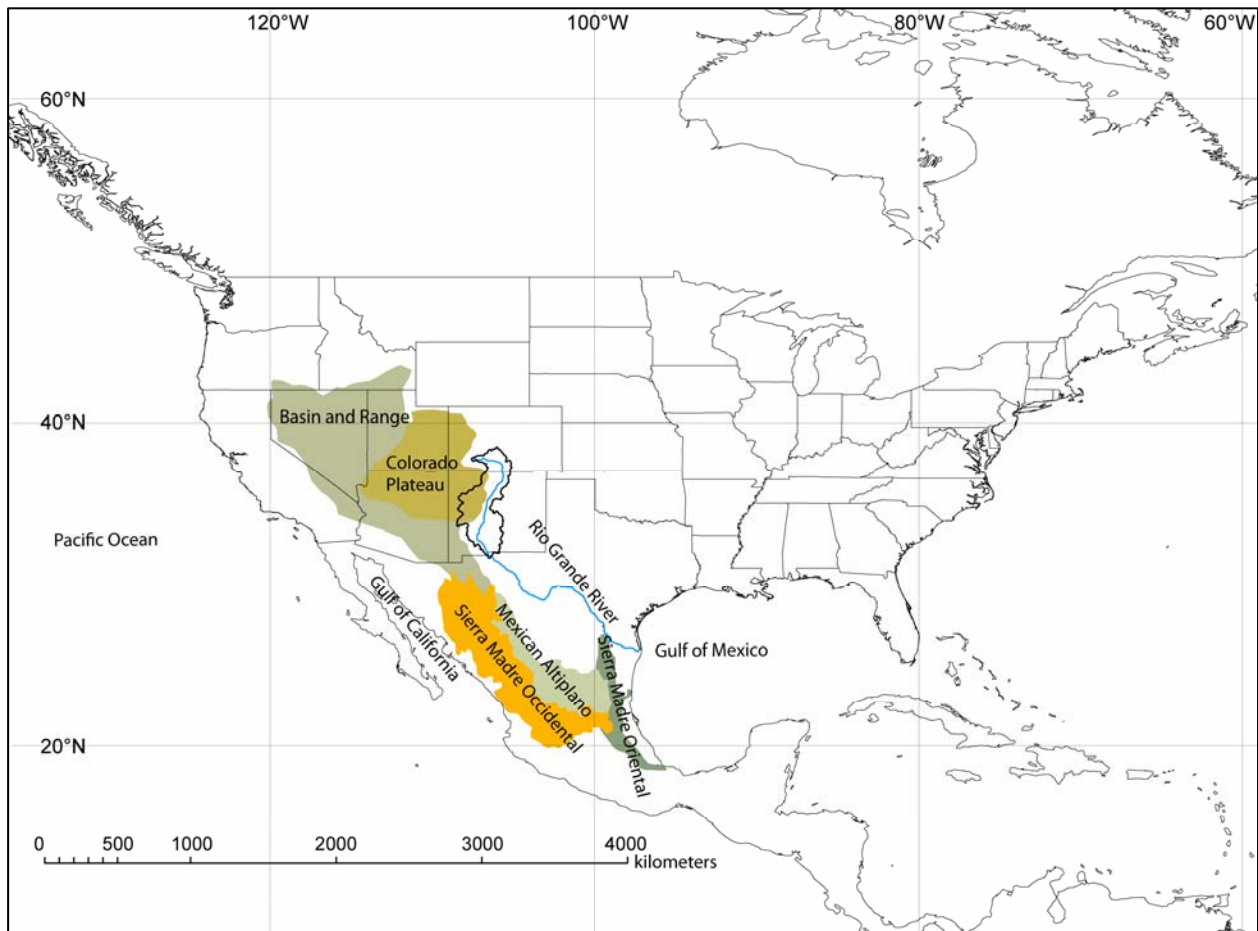


Figure 1. Index map of regional highlands and surrounding the portion of the Rio Grande watershed to be studied (delineated with bold black). Differential heating of the landmass and sea-surface creates unequal pressures that are equilibrated with monsoon winds. Drawn from USGS (2003) and Google Maps topography.

Douglas et al. (1993) gathered precipitation data from major regions in the U.S. and created annual histograms, sorted by month, for major cities in the southwestern U.S. Histograms with large precipitation levels in July, August, and September compared to the rest of the year are significantly influenced by the NAM. Douglas et al. (1993) demonstrate that the region most influenced by the monsoon is comprised of southern Arizona and New Mexico and north-central Mexico (figure 2).

In summary, the plateau of the western U.S. and Mexico creates a true monsoonal circulation pattern. A tongue-shaped air mass moves into Mexico and the southwest states starting in June, increasing until August and waning in September. This air mass is bounded to the north by dry air from the Pacific subtropical high. The monsoon is consistently centered over southwestern New Mexico and northern Mexico. With such large annual influence of the NAM over the Rio Grande River system, it is understood why changes in the NAM is postulated as a possible forcing mechanism for changes in sediment deposition in the delta system of the Rio Grande.

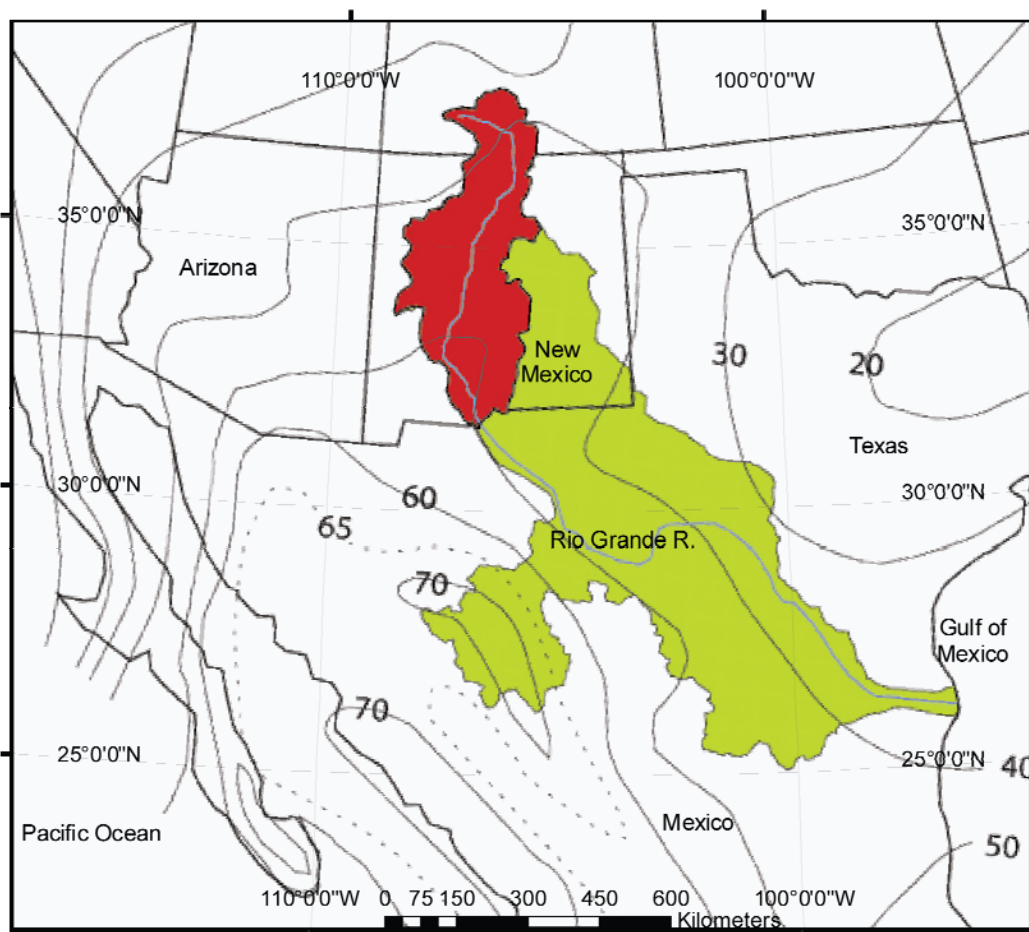


Figure 2. Red represents the portion of the Rio Grande River basin chosen for this study, and both red and green represent the entire watershed. Contours represent the percentage of annual precipitation received during the NAM months of July through August from 1931 to 1977. Figure adapted from Schmitt et al. (2004) and Douglas et al. (1993).

Rio Grande setting and history

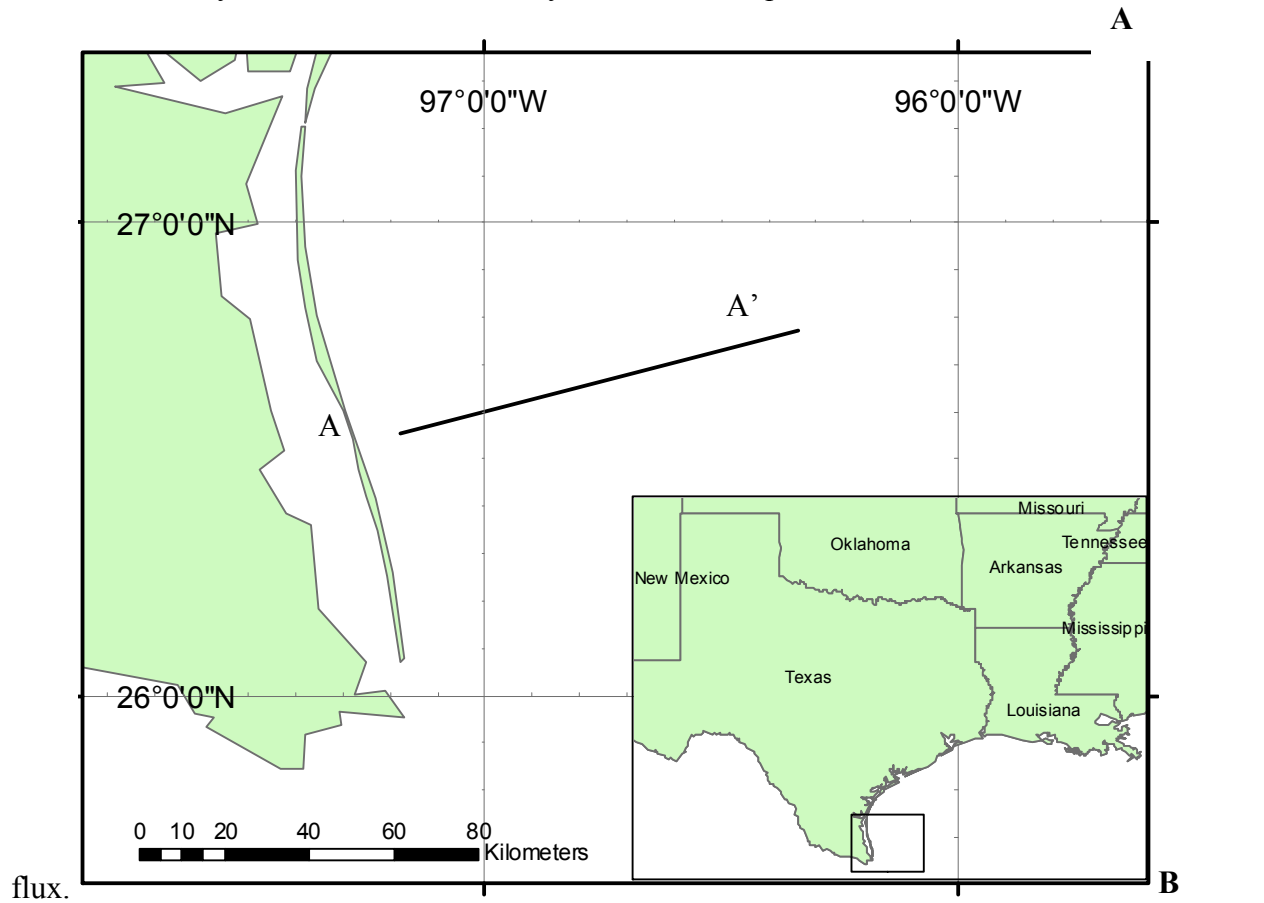
Entirely within the reach of NAM influence, the Rio Grande is one of the longest rivers in North America, flowing approximately 3025 kilometers from south-central Colorado to the GOM. The drainage basin that feeds the Rio Grande and includes the Pecos River is approximately 870,000 km². Historically, changes in relative base-level, hinterland tectonics, and regional climate have all significantly influenced the fluvial behavior of the Rio Grande. The development of the Rio Grande Rift during the middle Oligocene is the primary influence on formation and location of its axial Rio Grande River and drainage basin. From 5-0.8 Ma the Rio Grande River was largely in an aggradational state (deposition of sediment with no lateral movement of sedimentary facies), infilling its basins; and from 0.8 Ma to present the river behavior has been dominated by degradation (incision or erosion of sediment), during which time it incised into previously deposited fill. This more recent degradational period is represented by cycles of incision and partial backfill (Mack et al., 2006). These alternating phases of incision and fill are thought to be dominated by glacial-interglacial climate cycles. High river discharge and low sediment flux during glacial periods caused incision, and low discharge and high sediment flux during interglacial periods caused deposition (Mack et al., 2006). Despite extensional tectonic activity from 0.8Ma to present, the combination of base-level and climate dominated hinterland tectonic activity, as seen in fluvial sediment records (McMillian et al., 2006; Goldstein and Harrison, 1999; Mack et al., 2006). All three forcing mechanisms; including tectonics, base-level fluctuation, and climate change; have been dynamically influential on the river throughout its history. The Rio Grande delta provides abundant information about sediment deposition from the last glacial maximum, 21 ka, (LGM)

to present, suggesting the potential to examine the influence of climate forcing on that deposition.

Rio Grande delta

Work done to understand sequence stratigraphy in the Rio Grande delta has led researchers to believe that regional climate forced some depositional events from LGM to present. Seismic data were collected by Rice University's R/V Lone Star in order to see and understand the behavior of the Rio Grande River delta system (Banfield, 1998). Banfield (1998) analyzed the Rio Grande portion of the dataset and mapped out horizons of interest. Among the horizons, three regressive (progradational) units can be observed within the transgressive systems tract: 1B, 2B, and 4, deposited, respectively, in that order. TST 1B, 2B, and 4 show sedimentation that meets and exceeds sea-level rise (figure 3). Core is available from TST 1B and has been interpreted as a fluvially-dominated delta based on brown and gray silt overlain by sand and the prograding clinofolds seen in the seismic reflection profiles. Despite having no core for TST 2B, it has been interpreted, based on the seismic data, as an elongate fluvially-dominated delta. Horizons TST 1B and TST 2B are 11.5 and 9.5 ka old, respectively, approximated with the assumption that the entire thickness of the transgressive systems tract was deposited between 11.5 and 5 ka BP (Banfield, 1998). The youngest transgressive unit (TST 4) has been radiocarbon dated using mollusk shells at a minimum of ca. 5625 years (Berryhill et al., 1976) and has been interpreted as hemipelagic shelf mud (Banfield and Anderson, 2004). These three events evidence progradation during a period of overall eustatic sea-level rise, which would require either increased sediment deposition at the delta or periodic slowing, halting, or reversal of sea-level rise during this time interval (Lambeck and Chappell, 2001; Balsillie and Donoghue

2004. This study focuses on the sensitivity of increased deposition via monsoon-forced sediment



flux.

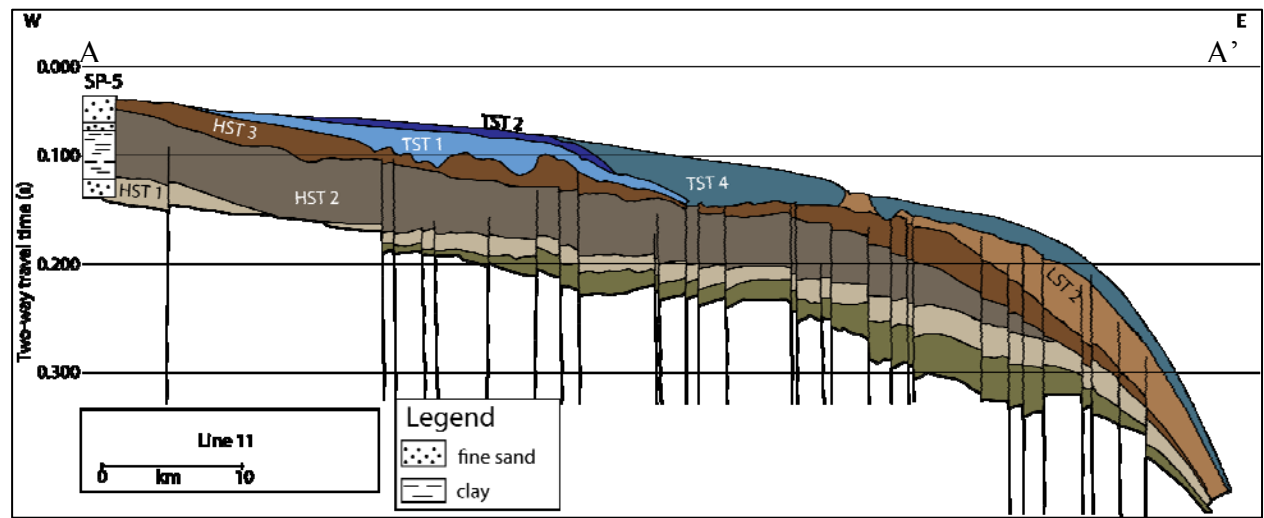


Figure 3. A. Map showing location of interpreted seismic reflection profile from A to A'. **B.** Interpreted seismic reflection profile of the upper-most units of the Rio Grande delta in the GOM. TST 2 is aggrading/prograding over TST 1, and TST 4 is extremely basin-ward, relatively. Tst 1B and 2B are included within TST 1 and TST 2, respectively. Image B replicated and colored from Banfield and Anderson (2004).

The purpose of this project is to determine if the NAM is a plausible forcing mechanism for increased sediment supply at the delta, which could then overcome the eustatic rise of sea-level during the last deglaciation phase of the climate cycle. During the time of deposition of TST 1 and 2, the estimated sedimentation was approximately $6.86 \text{ km}^3/\text{ka}$ (Banfield, 1998) at a time when sea-level was rising approximately 8 mm/a (Bard et al., 1996). Presumably this sediment load was transported to the delta when river flow was higher than present. Thus, flow conditions have changed within this short time span due to climatic influence. Blum (1994) suggested that summers dominated by a stronger maritime tropical air mass (i.e., the NAM) would cause a shift to high sedimentation from 11 ka to 5 ka BP. Poore et al. (2005) used GOM foraminifers, tree-ring thicknesses, and pack-rat middens to resolve monsoonal precipitation on a millennial time-scale and showed greater summer monsoon precipitation for 4.5-6.5 ka BP. This study will use climate change and monsoon variability to further extrapolate present sedimentation into the past.

Objectives

It is evident from seismic interpretation, carbon ages, and stratigraphic relationships (Banfield, 1998) that delta progradation overcame sea-level transgression multiple times between 11.5 and 5.5 ka BP. Monsoonal precipitation increase has been suggested as the cause of these prograding sediment lobes; however, this hypothesis needs validation by testing the sensitivity of sediment flux to changes in precipitation over the watershed. In order to complete this sensitivity test an understanding of the following is required:

1. Current relationships between stream discharge and suspended sediment load,
2. Effects of precipitation on stream discharge,

3. Variations of climate and its forcing mechanisms over the past 21 ka and related possible effects on precipitation.

Each of the above relationships will be discussed herein. The compilation of the three will be discussed in order to establish the plausibility of the NAM forcing progradation in the Rio Grande delta.

METHODS

Stream discharge-sediment relationship

Several concepts can describe the relationship between sediment flux and water discharge through a system. Stream discharge is directly affected by the velocity, width, and depth of the stream (Leopold and Maddock, 1953), which is shown by the equation:

$$Q=WVD, \quad (\text{Eq. 1})$$

where Q = discharge, W = width, V = average velocity, and D = depth. Hjulsrom (1939) showed that whether a grain of sediment is eroded, transported, or deposited depends highly on mean flow velocity. So it is evident that increased stream velocity must be associated with increased discharge when the channel dimensions remain constant. Increased discharge and flow velocity would therefore increase the sediment capacity of the system. Estimates of stream discharge, coupled with an empirical sediment equation gives a first-order look at potential sedimentation rates through time.

Sediment load can be estimated from stream flow by empirically deriving a sediment rating curve:

$$Q_s = pQ^j, \quad (\text{Eq. 2})$$

where Q_s is sediment flux, Q is water discharge, and p and j are unitless, empirically derived constants (Gordon et al., 2004). The constant j generally lies between 1.5 and 3, no matter what volumetric units are used (Knighton, 1984). Data from sediment stations within the watershed suggest p can range from single digits into the thousands. Suspended sediment data were taken from USGS stream gauge 08358300 at San Marcial, New Mexico because it is the most basinward sediment-stream gauge station within the study area with abundant data (Figure 4). Amin and Jacobs (2007) showed highest correlation between stream discharge and suspended sediment flux is found using the monthly sum of daily data. These stream gauge data agree that monthly sums show highest correlation. Using the monthly stream discharge and suspended sediment data from station 08358300, a sediment rating curve is derived to describe the sediment passing through this point of the Rio Grande River (Gordon et al., 2004):

$$Q_s = 2.14 * Q^{1.6}. \quad (\text{Eq. 3})$$

This equation approximates monthly sediment flux, in metric tons, using the sum of the daily

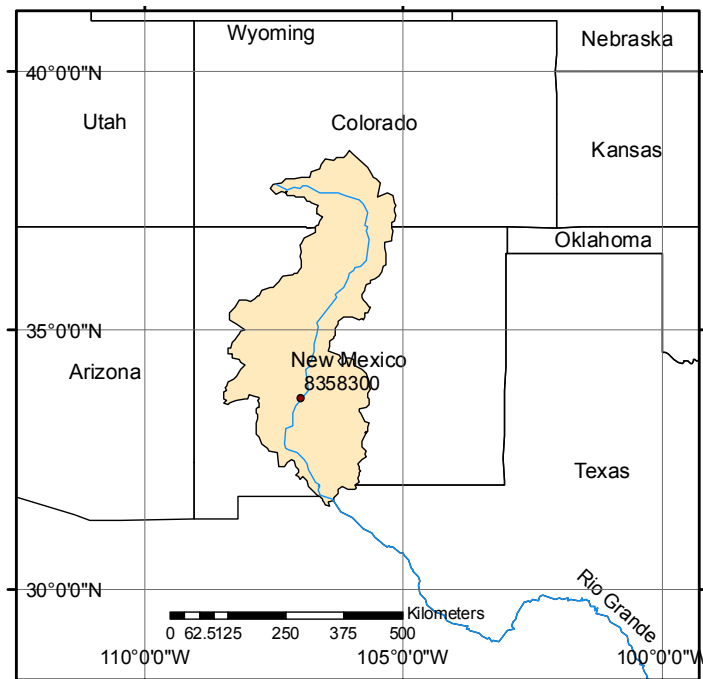


Figure 4. Location of the southernmost stream gauge, 08358300, which has the most complete stream record.

flow values for the entire month. Multiple stream gauges within the watershed were tested, each varying from the above equation. In general, other sediment stations showed larger values of p and j , therefore, equation 3 is a low-end estimate for suspended sediment flux. Estimating the relationship between sediment flux and water flux in the river makes approximation of sediment flux plausible.

Precipitation-stream discharge relationship

According to data collected from various stream and precipitation gauges within the watershed, the relationship between stream flow and precipitation is difficult to discern because of human controls in the system. Stream flow is controlled by 84 dams within the watershed (figure 5) and is drawn down by user withdrawal and irrigation. Total withdrawal, including groundwater and stream withdrawal, from the watershed is over 3 Ggal per day ($7886 \text{ m}^3/\text{s}$), and 1.8 Ggal/day ($4732 \text{ m}^3/\text{s}$) are withdrawn from surface water (Levings et al., 1998). Such high anthropogenic influence on water flux requires a model to roughly simulate stream discharge out of the watershed, had there been no population. Accurately simulating stream discharge within the watershed would require many more inputs than feasible for the scope of this project; therefore a simple (and less accurate) simulation will be used to determine magnitude of change, instead of actual flow differences.

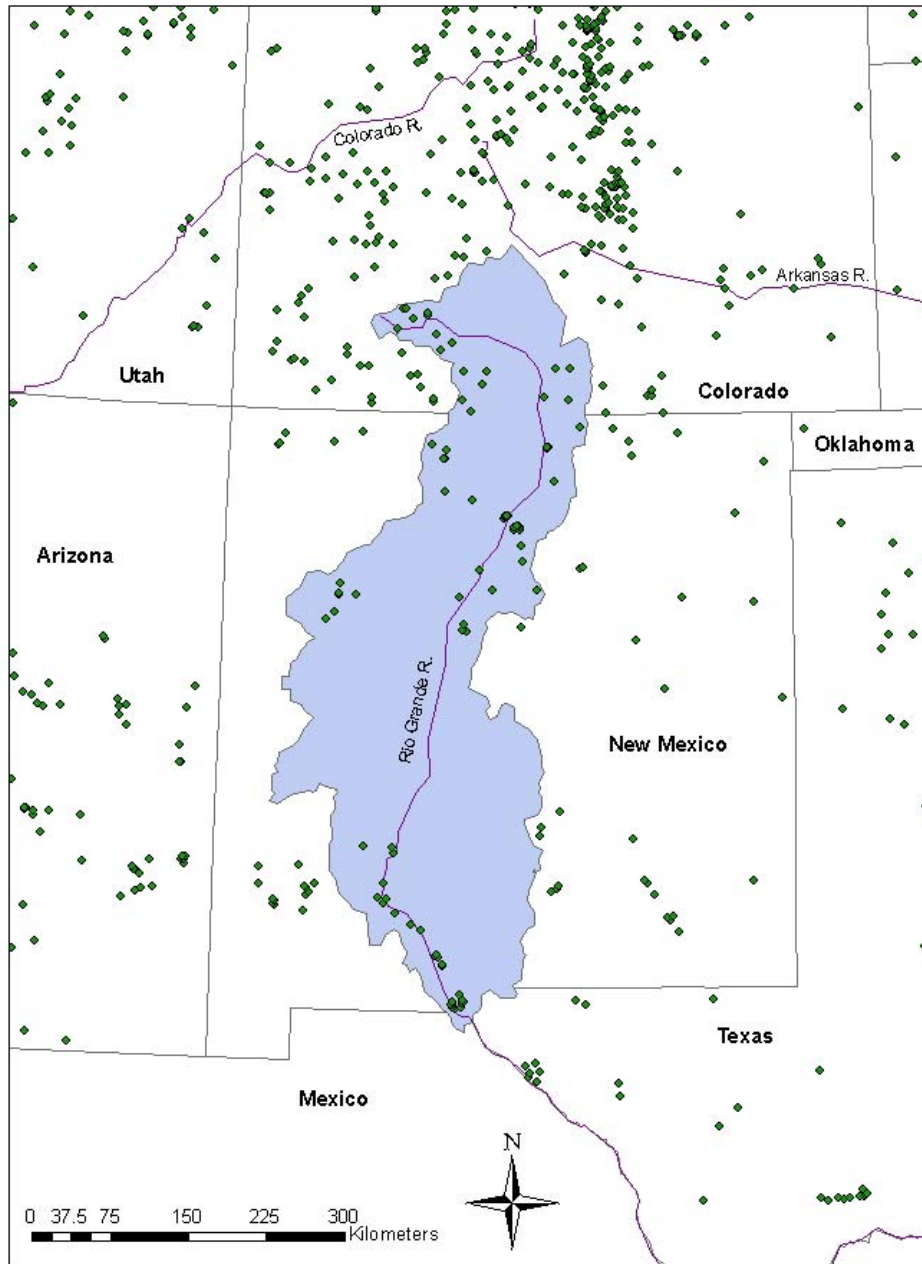


Figure 5. Eighty-four dams are contained within the New Mexico Portion of the Rio Grande Watershed (National Atlas, 2006); blue represents the watershed study area. High damming and manipulation of water blurs direct relationship between precipitation and stream discharge.

Watershed modeling

The simulation software used to approximate stream discharge through the watershed is Aquaveo's Watershed Modelling System 8.2 (WMS). WMS is used for its automated modeling processes, such as basin delineation, flow direction and accumulation processing, and geometric parameter calculation. Though these processes are automated, they require high computing power for a watershed project of this magnitude, so the digital elevation model (DEM) was scaled up by setting the output grid resolution to 250 m and exporting the data from ArcGIS. Resampling of input DEMs to 250 m grid spacing reduces computation time during watershed processing, yet still provides a reasonable demonstration of the tributaries and rivers within the watershed.

In order to create a hydrologic model using WMS, several processes were completed. The DEM was imported into the project with a UTM NAD 83, zone 13 projection. The DEM was then used to calculate flow direction and accumulation vectors. An output point (i.e. a point to which all upstream water flows, used to delineate the watershed) was chosen, the watershed delineated, and the model optimized by removing flow direction and accumulation data from the project file. The result is the basic template for a watershed simulation.

The runoff model used was the Army Corp. of Engineers' HEC-1. HEC-1 is a single-event modeling package that represents a watershed as an interconnected network of streams and sub-basins (HEC, 1998). The program outputs stream hydrographs by computing mathematical relationships between such parameters as slope, infiltration, and lag-time.

Additional parameters (i.e. timing of precipitation and runoff) were entered to tell the model how long to run and under what conditions. The model requires values, which specify what interval (minutes) to sample simulated stream discharge and how many samples to record.

Completed simulations are generally set to record samples of stream flow for a period of one month for continuity between simulation and recorded stream discharge values. Precipitation was entered into the model with a precipitation-time series, which describes the proportion of the total precipitation event with corresponding elapsed time. The precipitation values entered into the model were all basin-wide averaged simulated precipitation values from climate models, which are discussed hereafter. The loss method was defined as the Soil Conservation Service (SCS) curve number method, which is discussed in the curve number calculation section. WMS can compute the basin parameters and lag time for the watershed, which are also incorporated into the model. With all minimum parameters defined, the model was run and a stream discharge hydrograph was outputted. The mean values were extracted from hourly data in order to represent the mean flow value for each day.

Determination of watershed curve number

Simulation of storm runoff requires input to describe the ratio of infiltration to runoff for any given surface. The SCS curve number method is a simple and effective way to determine the amount of runoff for a given storm event. The SCS runoff equation is:

$$Q = \frac{(P - I_a)^2}{(P - I_a) + S} \quad (\text{Eq. 4})$$

Where Q = runoff; P = rainfall (in); S = potential maximum retention after runoff begins; and I_a = initial abstraction (i.e., water retained on surface due to vegetation, depressions in soil, evaporation, and infiltration (USDA, 1986))

The curve number is an empirical parameter used to predict runoff and infiltration during a given storm event. It is a function of soil type and land use. Soils can be separated into four

different hydrologic soil groups: A, B, C, and D, which experience more runoff from A to D. Land use also dictates the amount of runoff during a storm. Each land use code corresponds to individual descriptions (e.g., industrial, rangeland, or bare soil). The curve number is then found from the combination of land use and soil type and through referencing an empirical table (Table 1).

U.S. general soil map data were downloaded from the Natural Resource Conservation Service's National Cartography and Geospatial Center (Soil Survey Staff, 2002). Land use data (Price et al., 2001) were downloaded from the USGS Water Resources page. Land use was at a minimum during the mid Holocene. Ninety-five percent of the land within the watershed is primitive or rangeland, so the land use will be held constant for this basic model.

Individual zones of soil type and land use do not perfectly correspond. Therefore, they are intersected, creating separate zones, each having one land use code and one soil type. These are then assigned a curve number from Table 1 (figure 6). An area-weighted average curve number is then created by multiplying each area by its assigned curve number, summing all area-curve number products, and dividing by the area of the watershed of interest. For simulation purposes, the computed basin-average curve number is 69.7.

Table 1. Assignment of runoff curve number based on soil type and land use code

LU code	A	B	C	D	Description
11	54	70	80	85	Residential
12	89	92	94	95	Commercial and Services
13	81	88	91	93	Industrial
15	88	90	92	94	Industrial and commercial Complex
16	80	86	89	92	Mixed Urban
17	71	82	88	90	Other urban or built up land
21	49	69	79	84	Cropland and Pasture
22	43	65	76	82	Orchards, groves, vineyards, etc
23	68	79	86	89	Confined Feeding
24	62	74	82	86	Other Agricultural Land
31	39	61	74	80	Herbaceous Rangeland
32	44	64	77	82	Shrub-brushland rangeland
33	49	69	79	84	Mixed rangeland
41	30	55	70	77	Deciduous Forest Land
42	36	60	73	79	Evergreen Forest Land
43	43	65	76	82	Mixed Forest Land
51	100	100	100	100	Streams and Canals
52	0	0	0	0	Lakes
53	0	0	0	0	Reservoirs
61	44	58	68	75	Forest Wetland
62	32	55	68	75	Non-forested Wetland
71	25	25	25	25	Dry Salt Flats
73	25	25	25	25	Sandy Areas other than beaches
74	98	98	98	98	bare exposed rock
75	71	80	85	88	Strip mines, quarries and gravel pits
76	69	78	84	88	Transitional Areas
81	60	74	83	87	Shrub and brush Tundra
82	60	76	83	87	Herbaceous Tundra
83	77	86	91	94	Bare Ground
84	65	70	75	80	Wet Tundra
85	50	65	74	80	Mixed Tundra

(Price et al., 2001)

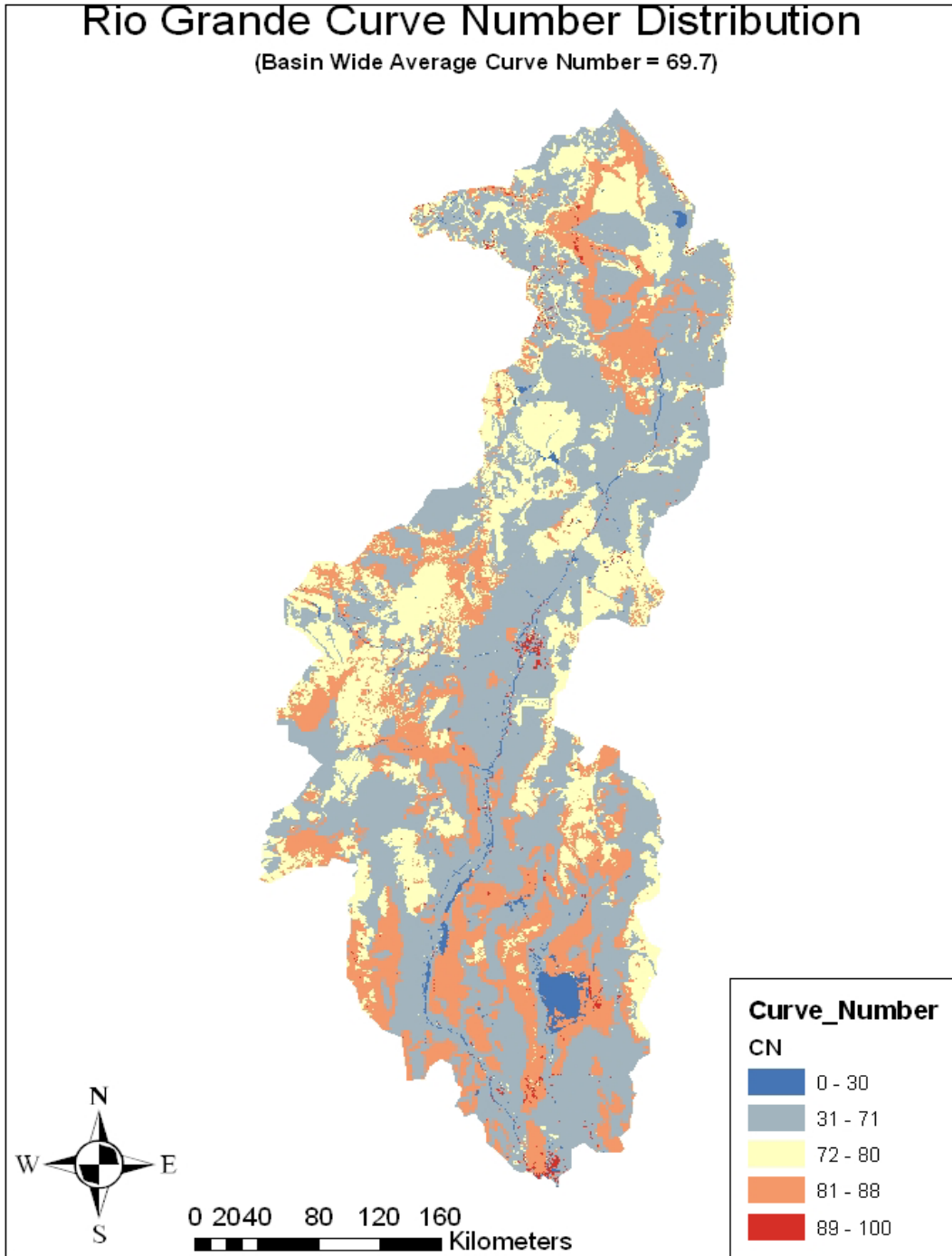


Figure 6. Distribution of curve numbers throughout the New Mexico and Colorado portion of the Rio Grande watershed. Higher curve number corresponds to higher river discharge for a given storm event.

Watershed models need a specific value entered for precipitation. This value may come from measured data such as rain gauges or from modeled data like the Parameter-elevation Regressions on Independent Slopes Model (PRISM) (PRISM, 2004) dataset. However, without

weather stations in the past, either proxy data or model data need be used to simulate potential watershed stream discharge.

Regional climate proxy data

Regional climate studies are abundant in the American Southwest and lend understanding to average annual effective precipitation, the precipitation remaining after runoff and evaporation. These studies include using calcite and aragonite layers in speleothems (Brook et al., 2006; Polyak et al., 2004; Polyak and Asmerom, 2001), mite species found in speleothems (Polyak et al., 2001), cave sediments (Applegarth, 1979), $\delta^{13}C$ analyses of eolian environments (Wilkins and Currey, 1999; Buck and Monger, 1999), lake levels and lacustrine $\delta^{13}C$ values (Wallace et al., 2009), faunal and needle investigations (Van Devender et al., 1987; Weng and Jackson, 1999), packrat midden studies (Van Devender et al., 1994; Coats et al., 2008; Holmgren et al., 2006), and tree-ring data (Euler et al., 1979) (Figure 7). Studies showing seasonal precipitation are less abundant. Among them, Holliday (1989) evaluated $\delta^{13}C$ values in bison bones to conclude that effective summer precipitation was reduced in west Texas from 7.5-5 ka. Poore et al. (2005) showed enhanced summer monsoonal circulation and precipitation from 4.5 to 6.5 ka BP. One study that confidently represents seasonal precipitation is a pollen study (Davis and Shafer, 1992), which describes wetter summer conditions from 8.5 ka to 21 ka BP and drier summer conditions from 4 ka to present.

The paleoclimate proxy studies show slight disagreement from 0 to 5 ka BP and 13 to 15 ka BP; however, they still give insight into average and some seasonal climate. The data generally show that average climate was drier from 5-10 ka BP, and wetter from 0 to 5 ka BP and 10-21 ka BP (Figure 8). Each of the three mentioned groups (0-5, 5-10, and 10-21 ka BP)

have at least 25% of the number of studies which disagree with the majority of each group, so the data may be inconclusive.

These proxy data give ground-based evidence for the general climate during various times in the American Southwest, but they do not give necessary information about how much precipitation is received each month, particularly during the monsoon months. Watershed models require exact quantities to describe precipitation, but the proxies only distinguish between ‘wetter’ and ‘drier.’ Because these data cannot be directly incorporated into the watershed model to simulate climate, simulation data must be created and employed. Therefore, general circulation models (GCM) are used.

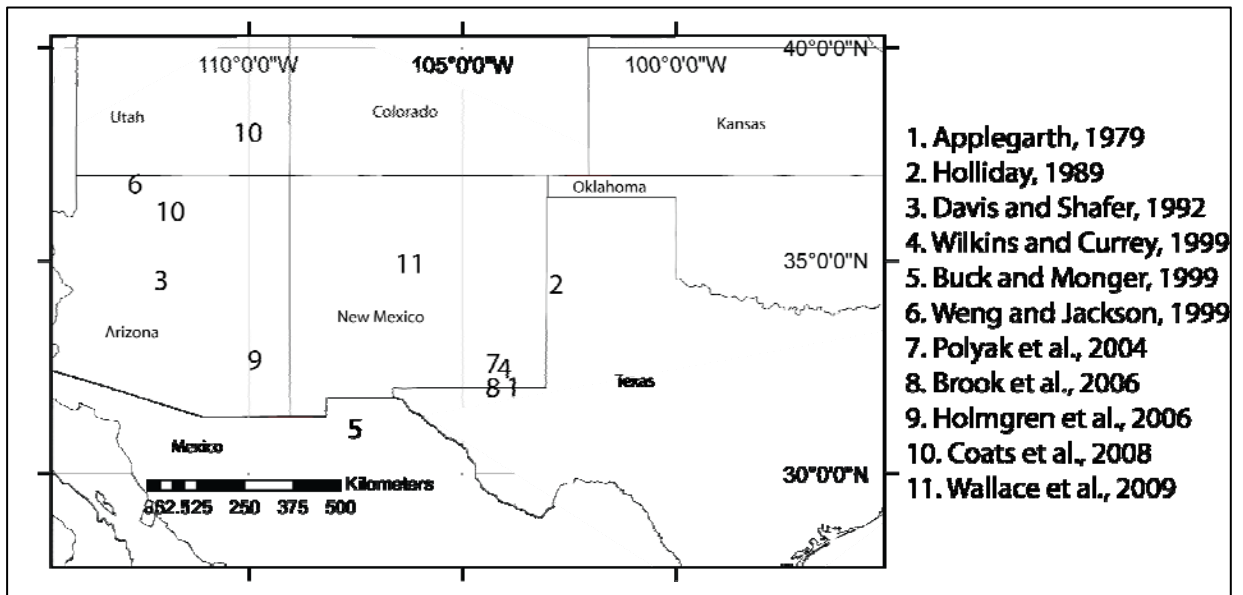


Figure 7. Locations of paleoclimate studies in the region. Though spread throughout the region, the proxy climate studies can yield general sense of climate from LGM to present.

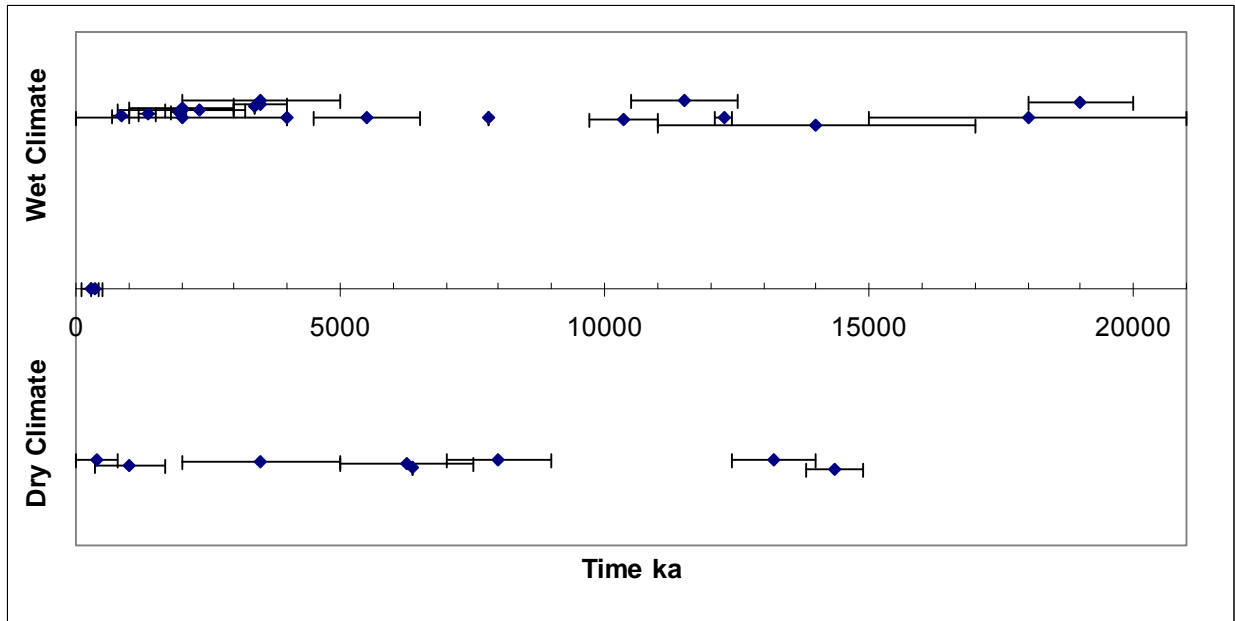


Figure 8. Index of climate wetness according to regional paleoclimate studies. Black bars represent the range of each study. Any study finding more effective precipitation than present was assigned to the ‘wet climate’ category and vice-versa. It can be generally inferred that climate was generally drier from 5-10 ka BP and wetter from 10-21 ka BP. Sources include all those listed in figure 7, plus Poore et al., 2005.

General Circulation Models

GCMs simulate aspects of climate using equations and information that describe the circulation of energy around Earth and conditions therein. Boundary conditions; such as land mass extent, topography, solar intensity, greenhouse gases, and ice-sheet extent; can be adjusted to simulate climatic patterns at various times. The Paleoclimate Modeling Intercomparison Project (PMIP) is a group of climate modelers who have united to share data and outputs of simulations. These data collectively provide a powerful view into past climate because the suite of models can be used in combination to understand climate. The PMIP suite models the climate of three time periods: The 0 ka control run, the 6 ka solar intensity test, and the 21 ka Glacial Maximum. Knowing the boundary conditions for the models can help to highlight their usefulness in understanding monsoonal influence on sediment flux in the Rio Grande.

Boundary conditions

The suite of PMIP2 GCM's is designed such that each of the models shares the same boundary conditions for a given time interval. The boundary conditions are the inputs for any one model with which the model is then set to run a predetermined number of time steps to simulate a dynamic climate. Each model must have a pre-industrial control run to determine its usefulness and applicability for further runs, into the past or future. Following the control, runs are completed to simulate 6 ka and 21 ka world climate as well. The boundary conditions apply to the coupled ocean-atmosphere GCM's and are shown in Table 2 (Braconnot et al., 2007).

Table 2. Boundary conditions for the PMIP 2 models: 0 ka and 6 ka

		0 ka	6 ka
Topography, coastlines		Modern	Modern
Ice Sheet Extent		Modern	Modern
Green House Gases	CO₂	280 ppm	280 ppm
	CH₄	760 ppb	650 ppb
	N₂O	270 ppb	270 ppb
	CFC	0	0
	O₃	Modern 10 DU	Modern 10 DU
Insolation	Solar Constant	1365 W/m ²	1365 W/m ²
	Eccentricity	0.016724	0.018682
	Obliquity	23.446 °	24.105°
	Angular Precession	102.04 °	0.87°
Initial Ocean State		Warm Ocean State	Warm Ocean State

Because the Rio Grande delta progradational events happened at approximately 6-11ka, the 6 ka model will be the model suite of choice for this study. As compared to present day, the two boundary condition changes for the 6 ka BP model are solar radiation (due to changes in Earth's orbit around the sun) and atmospheric methane (Table 2). Though methane concentration in the atmosphere differs by -14% between 0 ka and 6 ka BP models, it is a small radiative change by comparison to the changes in solar radiation (Kiehl and Trenberth, 1997,

Braconnot et al., 2007). Therefore, climate change 6 ka BP as compared to present day is dominated by the changes in solar radiation (Rupper et al., 2009).

Insolation

The 6 ka run is a sensitivity test to the biggest differences in insolation as orography and coastline extent is held constant, with slight changes in greenhouse gases. This change in solar insolation is forced by changes in Earth's orbit around the sun. Specifically, the changing values of eccentricity, obliquity, and angular precession through time dynamically influence the solar radiation received at Earth's surface (Table 2). Berger (1992) derived solar insolation at various latitudes, which differ because of tilt. Thirty degrees north latitude is closest to the study area, which lies just south of the Mexican border. The solar radiation received at 30°N during June for each 1000 year time step is also described in Table 3 and is plotted in figure 9. At this scale, the solar radiation received from the sun is dictated mainly by the location of the equinoxes along the elliptical orbit (i.e. precession).

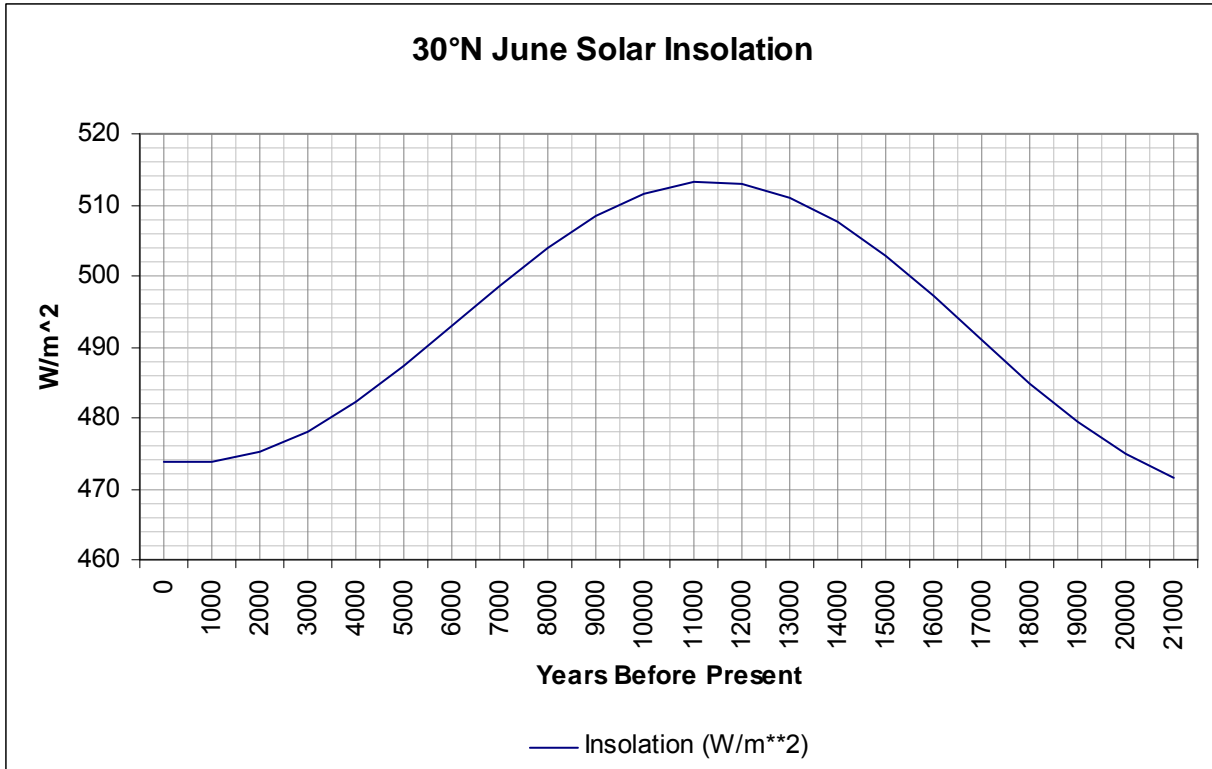


Figure 9. Insolation from the sun during June at 30°N on Earth's surface. This increase in summer energy could potentially increase monsoon intensity (Berger, 1992).

Table 3. June insolation values at 30°N latitude (Berger, 1992)

Years BP	Insolation (W/m**2)	Eccentricity, ϵ	ω	Obliquity °	Precession: $\epsilon \sin \omega$
0	473.93	0.017236	101.37	23.446	0.0169
1000	473.77	0.017644	84.26	23.573	0.01756
2000	475.14	0.018024	67.23	23.697	0.01662
3000	477.99	0.018376	50.3	23.815	0.01414
4000	482.12	0.018697	33.45	23.923	0.01031
5000	487.23	0.018988	16.68	24.019	0.00545
6000	492.9	0.019249	359.99	24.1	0
7000	498.66	0.019477	343.37	24.163	-0.00557
8000	503.99	0.019674	326.82	24.206	-0.01077
9000	508.44	0.019839	310.32	24.229	-0.01513
10000	511.6	0.019971	293.86	24.229	-0.01826
11000	513.16	0.020071	277.45	24.207	-0.0199
12000	512.98	0.020139	261.07	24.161	-0.01989
13000	511.06	0.020175	244.71	24.093	-0.01824
14000	507.55	0.02018	228.37	24.004	-0.01508
15000	502.75	0.020154	212.04	23.895	-0.01069
16000	497.05	0.020098	195.71	23.769	-0.00544
17000	490.94	0.020012	179.38	23.627	0.00022
18000	484.89	0.019898	163.04	23.475	0.0058
19000	479.38	0.019756	146.69	23.315	0.01085
20000	474.82	0.019589	130.34	23.151	0.01493
21000	471.52	0.019398	113.98	22.989	0.01772

It is expected that insolation will directly affect monsoonal intensity. The intense summer insolation is the forcing mechanism of the monsoon. As it heats up the continent, a low-pressure ridge forms, which changes atmospheric circulation and wind patterns. Therefore, if the summer insolation is more intense 6 ka BP, as seen in figure 9, the monsoonal effect will potentially be more intense. Increased monsoonal intensity potentially increased monsoonal precipitation.

GCM data

The PMIP models were run at various grid cell resolutions, ranging from 2.8125 to 5.625 decimal degree squares (243-625 km longitudinal distance). This project focuses on an area that could fit almost entirely inside of one or two grid cells, therefore, six models with the finest grid

cell resolution were chosen. The PMIP 2 models used for this portion of the study are listed as follows:

- CSIRO Mk3L climate system model, version 1.1: Australian Commonwealth Scientific and Industrial Research Organization, Australia
- ECHAM5-MPI OM 1: Max Planck Institute for Meteorology, Germany
- FGOALS-1.0g: Institute of Atmospheric Physics, Chinese Academy of Sciences
- MIRO 3.2- Center for Climate System research, National Institute of Environmental Studies, Frontier Research Center for Global Change, Japan
- MRI-CGCM 2.3.4fa- Meteorological Research Institute, Japan
- UBRIS-HadCM3M2- University of Bristol, United Kingdom

Temperature and precipitation output from each model were extracted for two zones: a northern zone which surrounds the study area in the US southwest and a southern zone that encompasses the area in northern Mexico where the majority of annual precipitation is received during the monsoon months. The northern zone data were extracted if the top left corner of the cells lay within latitudes 30° and 38.5° N and longitudes 113° and 101° W, and the southern zone data were bounded by latitudes 30° and 19.8° N and longitudes 113° and 95° W (figure 10). These large areas lack precision for an area the size of the Rio Grande watershed, but these data will capture shifts in climate from one time to another.

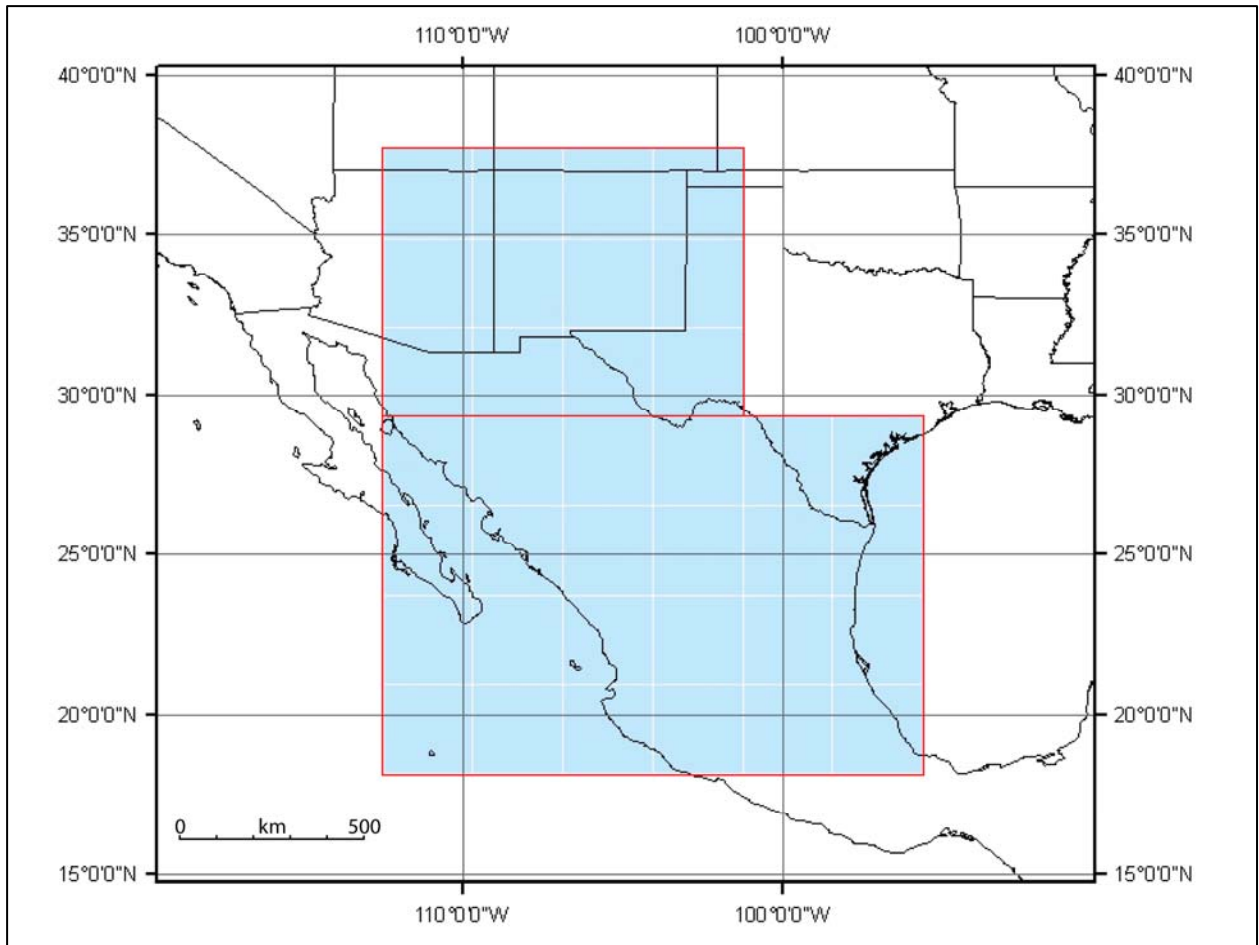


Figure 10. Locations of extracted grid cells for the MIRO model run. The MIRO model exhibits the smallest, and most common grid cell resolution of 2.1825 decimal degree squares, but some of the models have larger grid cell resolutions. The smaller, upper group of cells was extracted and averaged together, and the same is true for the larger, southern group of cells.

GCM results

Each of the model outputs of precipitation and temperature were averaged together for every month, and one standard deviation from the mean was considered as the margin of error. The 0 ka control run temperature output closely matches the seasonal trends observed in present climate. Both northern and combined cell block areas show seasonal warming to a peak average of 24°C during July and the upper and combined cell block areas have a winter low in January of

-1°C and 10°C, respectively. The 0 ka GCMs are relatively precise in temperature measurements, having an average standard deviation between months of 1.9°C.

The precipitation outputs of the GCM's also match trends of the present day. The models predict dual peak precipitation: late winter experiences minor precipitation compared to the summer monsoon months, when proportionately more precipitation is incurred (figure 11). The PRISM climate data, extracted for the watershed, show that 43% of annual precipitation is received during months July-September. The north cell block average precipitation shows that 29% of the annual precipitation is received during the monsoon season. This discrepancy between the PRISM data and the GCM data is most likely due to the smaller region of the watershed when compared to the greater region of the upper cell block. Monsoonal precipitation in the southern cell block more greatly affects annual precipitation because the monsoon influence is stronger in northern Mexico, as observed in figure 2. Despite discrepancies between GCM data and PRISM data, we expect the GCM data to capture climate trends reasonable well for our purposes.

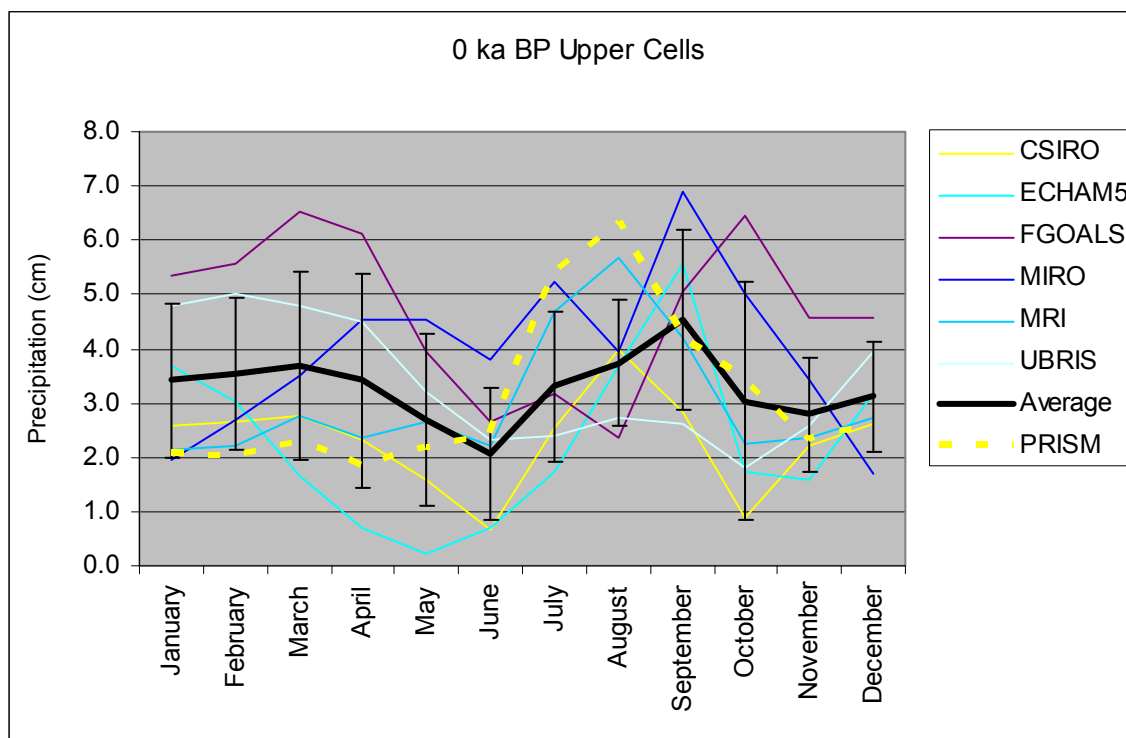


Figure 11. 0 ka GCM precipitation simulation for the upper cell block with monthly model standard deviation attached to the average trend line. Error bars represent each month’s standard deviation above and below the mean. Note the similarity between the ground-truth based PRISM climate data and the GCM Average.

The 6 ka model outputs differ from the control run. The difference between the paleoclimate simulations and the 0 ka control run can be used to discover any precipitation or temperature anomalies over the region for 6 ka BP. Variance of model data can be gauged using this simple formula:

$$\text{Index of variability} = \frac{\sigma_P}{\Delta P} \text{ or } \frac{\sigma_T}{\Delta T} \quad (\text{Eq. 7})$$

where σ is the standard deviation between models, p is precipitation, μ is the average of all model outputs, and T is temperature, all for a given time period such as a certain month (Rupper and Koppes, 2010). If the index of variability is less than 1, the models have changed less than the standard deviation between the models; therefore, they are in concurrence with each other. If variability is greater than or equal to 1, the average change is more than the standard deviation,

thus the models disagree. Model concurrences may show stronger confidence for particular months.

The average monthly temperature results for the 6 ka model runs are consistent with each other; the index of variability is less than one for most months. The 6 ka run shows that months July through October are warmer than corresponding months in the control run and months November through June are colder than the 0 ka run (Figure 12). The warmer summer/fall is easily explained by the solar insolation boundaries set on the 6 ka run (see solar insolation section).

Model precipitation outputs are more variable than temperature. This is because precipitation is more dynamically influenced than temperature. Such high magnitude of

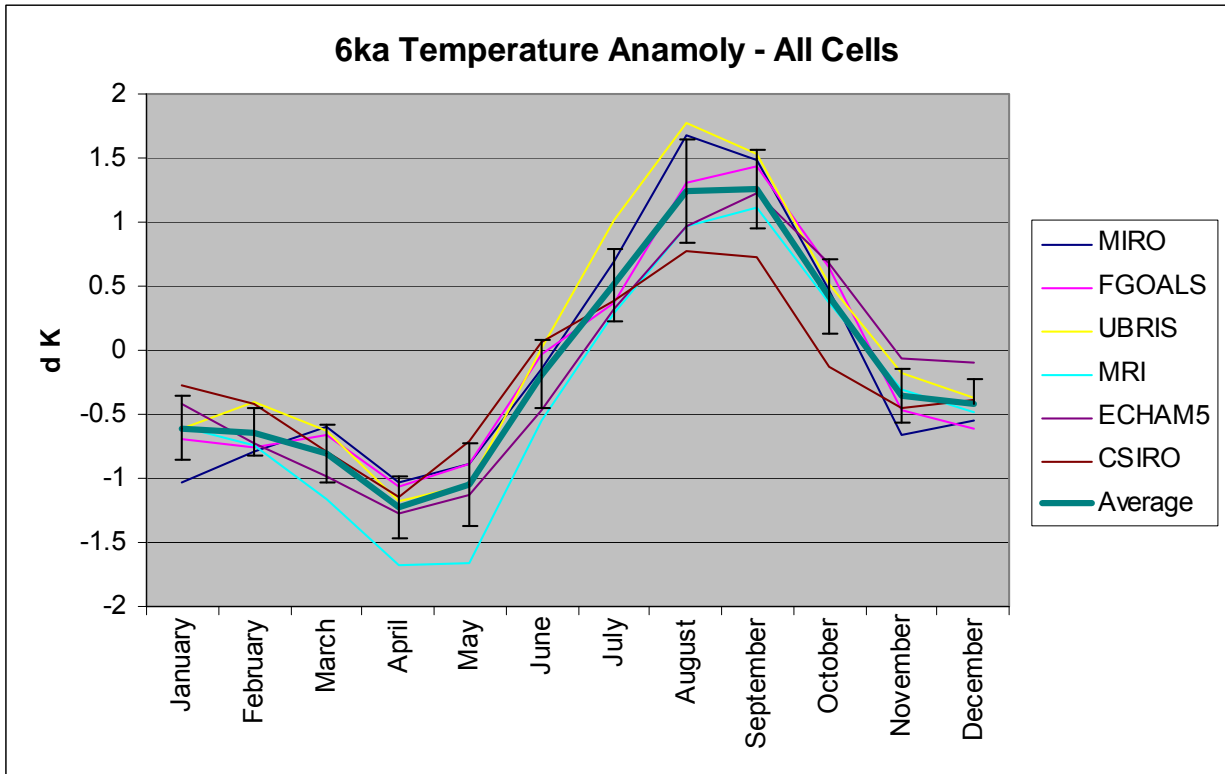


Figure 12. Temperature anomaly for 6 ka model runs. Direction and magnitude of each model is consistent with the rest. July through October is warmer than the present, which could generate greater monsoon intensity than the present.

variation is confirmed by using the index of variability equation, which shows that they vary highly. Observing trend direction between models during monsoon months can also be used to evaluate monsoonal influence. Of the six models in the upper region, four show increased precipitation during the monsoon months. The same is true for the average of both the upper and lower regions. Though magnitudes may differ, the majority of models show that summer monsoonal precipitation was higher 6 ka than for the present (figure 13). Though the index of variability show high variance between monthly model precipitation data, the consensus between the models shows heightened summer monsoon precipitation 6 ka BP.

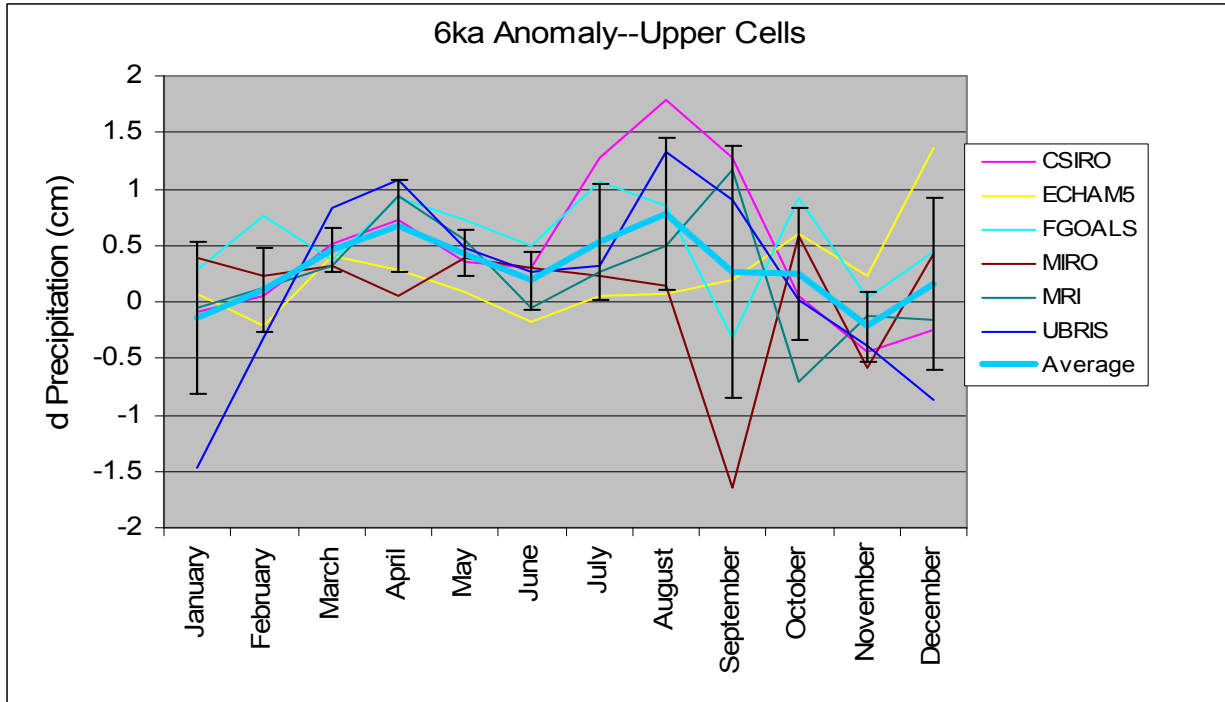


Figure 13. Average monthly precipitation anomaly for 6 ka, the bold black line representing the average of plotted models and error bars representing the monthly standard deviation. Winter months are drier and spring and monsoon months are wetter than the 0 ka model.

The results of these models provide a valuable link between known parameters, such as solar intensity, and the watershed model. Though the models do not fully agree, directional trends between them are discernable. The average of the models can be used as the main precipitation inputs into the watershed models because the quantitative precipitation values are given in cm/month, where paleoclimate proxy data only gives qualitative change in precipitation. Thus, the GCMs quantify what the proxy data show as only ‘wetter’ or ‘drier’ trends.

GCM results and paleoclimate proxy data

Results of the GCM precipitation data show that precipitation during the monsoon season is heightened 6 ka BP. Presumably, the heightened insolation received at this time increases monsoonal effect, thus increasing precipitation during the summer monsoon months. As expected, GCM results also show heightened summer temperatures for this time. With the

paleoclimate proxy data in general agreement that the climate was drier and the GCM's showing heightened monsoonal precipitation, questions arise regarding which is correct. Both scenarios can be correct. Hotter climate will experience more evaporation, but can still facilitate stronger monsoons. Therefore, drier summers would be punctuated by short bursts of intense monsoonal precipitation. Understanding the relationship between empirical data and simulation data leads to better understanding of the climate for 6 ka and, presumably, for 9.5 and 11.5 ka. Testing the 6 ka GCM data against 0 ka GCM data will require knowledge of monsoonal storm statistics.

Storm frequency and concentration

Frequent storms vs. constant precipitation

Given a fixed amount of precipitation per storm over the watershed area, the timing of the precipitation affects the peak stream discharge value. A simple experiment was performed using the watershed model to understand this relationship for a hypothetical 10-day storm. Two trials were performed, each assuming 2.54 cm of precipitation over the entire watershed. The first trial used a linear cumulative precipitation curve and the second used a 10-day curve in which three linear 24 hour storms occurred, each comprising one third of the total precipitation for the ten days. The resultant two curves show that the multi-event, 10 day precipitation period produces a larger peak stream discharge (figure 14) than the constant precipitation.

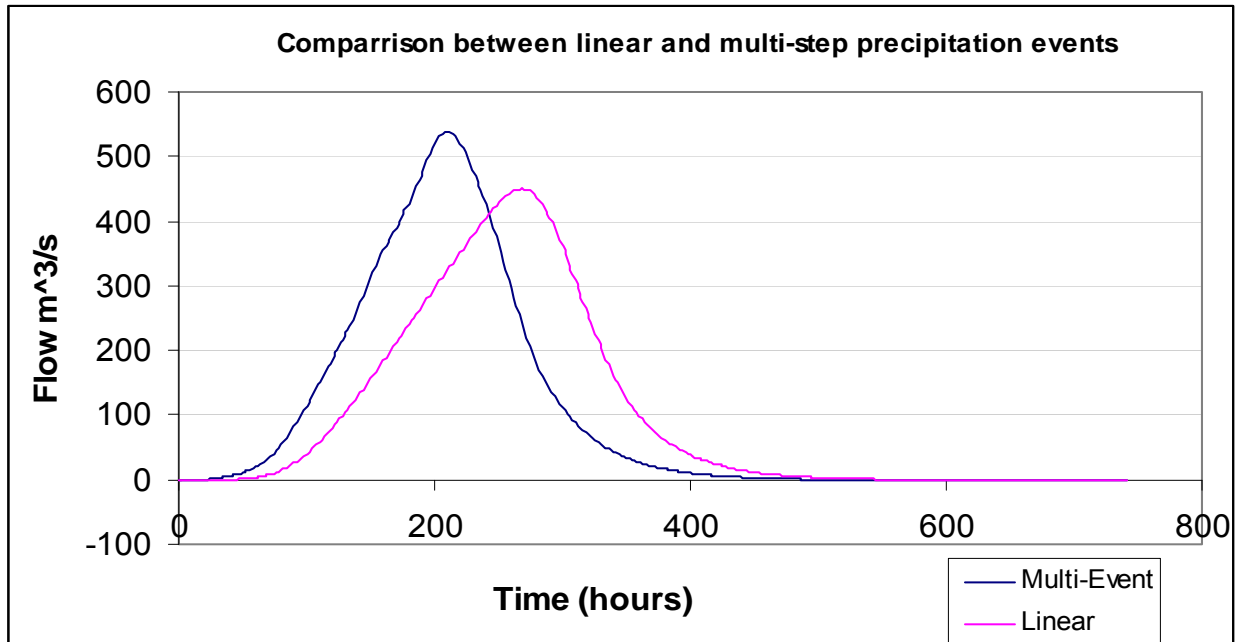


Figure 14. Comparisons of multi-event, 10-day storm versus constant 10 day precipitation. The multi event produces higher peak flow because of larger bursts of precipitation. Although natural storms do not produce linear cumulative-time curves this is important to consider when modeling the watershed because frequency greatly impacts peak suspended sediment flux.

Regional storm concentration

Understanding the average duration of storm events in each month for the region is important to watershed modeling, where the average monthly rainfall is used for the precipitation input. The monthly precipitation averaged over the entire watershed can be divided by the average number of events experienced in the watershed in a given month to more closely approximate stream discharge. To statistically determine the approximate length and recurrence of precipitation events in the region the 10 longest precipitation gauge records were selected. Not all of them are within the defined New Mexico portion of the Rio Grande watershed, which is acceptable, given the course resolution of the paleoclimate models (figure 15).

In order to determine the quantity of storms occurring in the region per month, first a definition for a storm event must be made. It is defined here as any number of consecutive days above the monthly average where precipitation is recorded. This definition works within this

desert setting due to the low daily average precipitation (many days incur no precipitation at all), so any notable event will be a day above monthly average precipitation. For each month and station the total number of precipitation events was determined (Table 4).

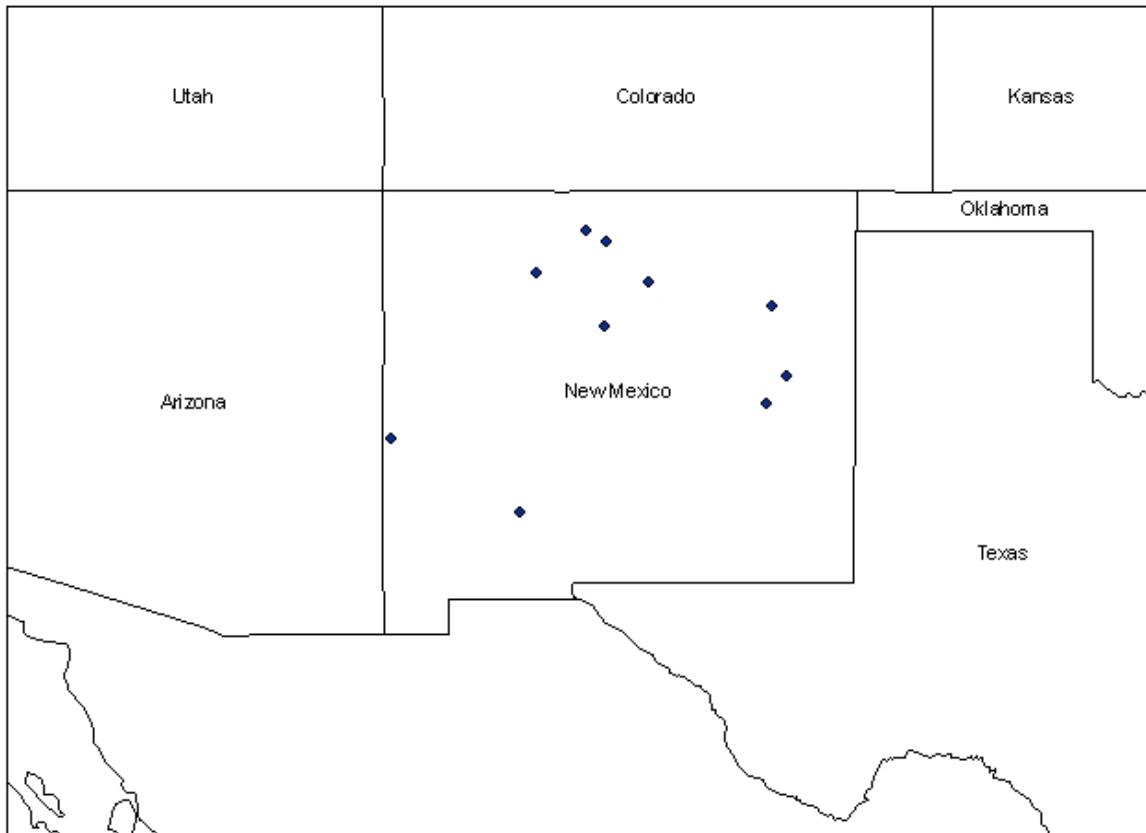


Figure 15. Locations of the rain gauges for the longest running precipitation records within the state of New Mexico.

The results of this simple survey show that rainstorm duration does not significantly increase during the monsoon months of July through September, as compared to the annual average rainstorm duration. However, the quantity of storms does increase by almost double (Table 4). The duration of the storms does not vary much from winter to summer and does not stray far from 24 hours (the average duration is 1.4 days, closer to 24 hours than 48 hours), thus the pre-

defined 24-hour Type-II curve (figure 16) can be employed to best simulate the rate at which the total precipitation is accumulated over the watershed.

Table 4. Average days per storm and average storms per month

Month	Average Days/Storm	Average Storms/Month
Jan	1.36	2.51
Feb	1.34	2.53
Mar	1.38	2.54
Apr	1.4	2.2
May	1.49	2.44
Jun	1.42	2.58
Jul	1.47	4.42
Aug	1.44	4.5
Sep	1.49	3.07
Oct	1.51	2.44
Nov	1.4	2.1
Dec	1.36	2.44

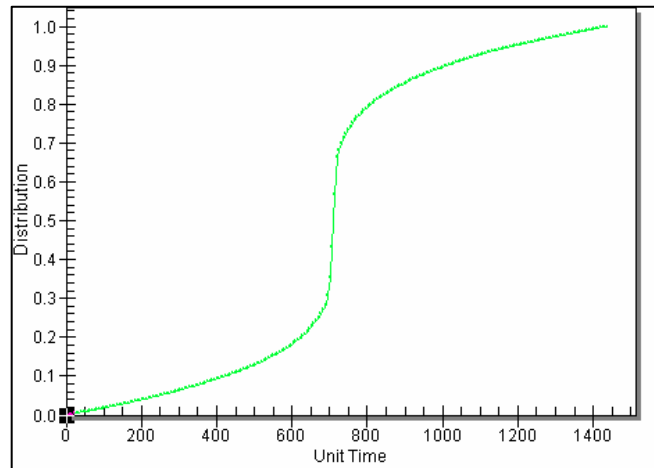


Figure 16. The Type-II 24 hour curve as defined in the WMS software. Distribution is defined as the cumulative percentage of total accumulation and unit time is in minutes.

This affects the modeling method by making the type II 24-hour curve applicable to each modeled storm event and necessitating division of the total monthly precipitation into the number of storm events modeled for a month. With this knowledge, 0 ka stream discharge is simulated using the current known storms/month; however, the storm frequency during 6-11 ka is unknown, so a sensitivity test will also be performed. This test will add and subtract 50% frequency for each monsoon month to see if the monsoon precipitation can still explain the pulses of sedimentation.

Sediment simulation

A first order test using simulated stream discharge values outputted from the watershed model was completed to demonstrate the change in direction of sediment flux which could be experienced from 0 ka to 6 ka. This was accomplished by first making assumptions about how many storms occur each month. This study assumes possibly 4 storms occur each month (no change from the modern) but tests 2 and 6 storms per month to see how that would affect the results. The simple watershed model requires only a basin-wide average precipitation value. GCM cell values outputted from the upper and the average of the upper and lower cell blocks were used for this precipitation value. The GCM precipitation values were divided by the number of storms per month. The watershed model was designed to sample flow measurements every two hours, which measurements were averaged into mean daily values and summed into monthly discharge values. The monthly discharge was then multiplied by the respective number of days per storm for an approximate monthly total. The flow values were inputted into equation 3 for a total suspended sediment flux during the simulation. This process was repeated using precipitation values both one standard deviation above and below the mean modeled

precipitation. These values are plotted (figure 17, Table 5) to show the absolute and percent difference in sediment between 0 ka and 6 ka simulations. It is important to note that this method underestimates stream discharge as it assumes now overlap between storm events.

The tests show that when the GCM precipitation average value is used as precipitation input, increased suspended sediment flux is experienced for all runs. Results for the 4 storm per month test, using the upper cell precipitation values show an increased suspended sediment flux out of the watershed of 79%, averaged from July-September. Tests using the 4 storm per month precipitation values of the total cell average show increases in sediment flux of 45%, averaged from July-September. The 2 storm per month tests are higher and the 6 storm per month test lower, the effects exaggerated because of the exponential relationship between stream discharge and sediment flux. Tests where one standard deviation above the mean precipitation was entered show even higher sediment increases. However, if the monsoonal precipitation is actually one standard deviation below the mean modeled precipitation, increases are only observed for the 2 storm per month tests.

6ka Sediment Flux, Compared to 0ka

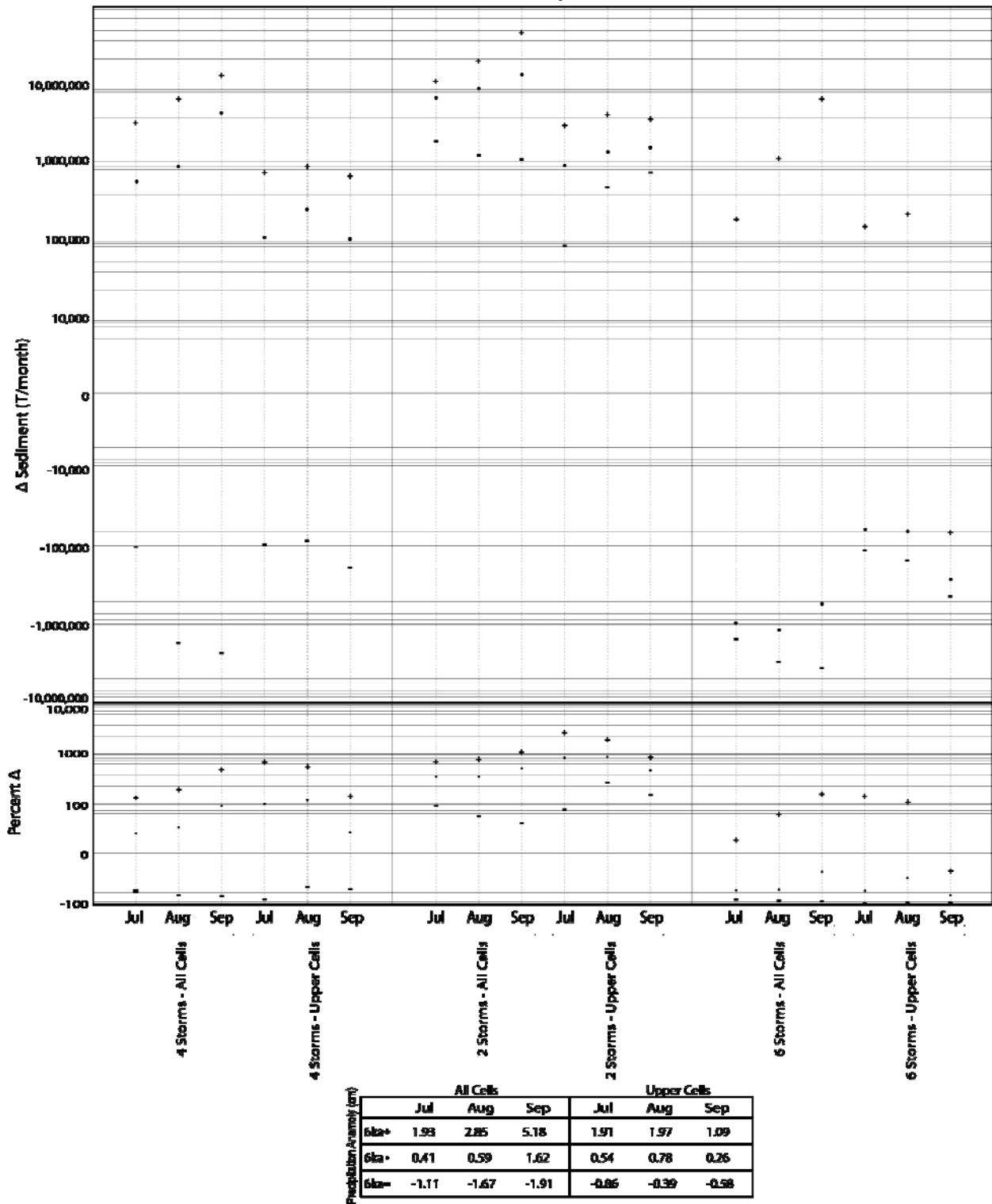


Figure 17. Plot of 6 ka-0 ka simulated suspended sediment flux and the percent difference based on the three experiments: 4, 2, and 6 storms/ month. The average (•) and average plus (+) and minus (-) one standard deviation are plotted.

Table 5. Sediment experiment runs with precipitation input, raw sediment values, net difference, and percent difference

	6ka GCM4		6ka GCM2		6ka GCM5	
Average Precipitation	GCM All Cell Average	GCM Upper Cell	GCM All Cell Average	GCM Upper Cell	GCM All Cell Average	GCM Upper Cell
Simulated 6ka Sediment (T/month)	247862.9	386795.2	6528728.4	209866.2	402153.5	507897.8
Control 0ka Sediment (T/month)	2019542.3	3013809.0	3557785.9	108599.8	182967.0	409430.9
6ka Sed0ka_SedJ	0.2	0.3	0.8	0.9	1.2	0.2
%difference	22.7	28.3	83.5	93.2	119.8	24.0
6ka-0ka	459020.6	853986.2	2970942.5	101256.3	219186.4	98466.8
Average+Standard Deviation	6ka GCM4		6ka GCM2		6ka GCM5	
	GCM All Cell Average	GCM Upper Cell	GCM All Cell Average	GCM Upper Cell	GCM All Cell Average	GCM Upper Cell
Simulated 6ka Sediment (T/month)	4717209.2	857128.8	17516838.0	711826.3	989572.7	944349.0
Control 0ka Sediment (T/month)	2019542.3	3013809.0	3557785.9	108599.8	182967.0	409430.9
ratio	1.3	1.8	3.9	5.6	4.4	1.3
%difference	133.6	182.6	392.4	555.5	440.8	130.6
6ka-0ka	2697867.0	5503319.8	13959052.1	603226.4	806605.6	534918.0
Average+Standard Deviation	6ka GCM4		6ka GCM2		6ka GCM5	
	GCM All Cell Average	GCM Upper Cell	GCM All Cell Average	GCM Upper Cell	GCM All Cell Average	GCM Upper Cell
Simulated 6ka Sediment (T/month)	1077292.3	1275457.6	1395192.0	24505.3	113185.0	234185.6
Control 0ka Sediment (T/month)	2019542.3	3013809.0	3557785.9	108599.8	182967.0	409430.9
ratio	-0.5	-0.6	-0.6	-0.8	-0.4	-0.4
%difference	-46.7	-57.7	-60.8	-77.4	-38.1	-42.8
6ka-0ka	-942250.0	-1738351.4	-2162593.9	-84094.5	-69782.0	-175245.4
	6ka GCM4		6ka GCM2		6ka GCM5	
	GCM All Cell Average	GCM Upper Cell	GCM All Cell Average	GCM Upper Cell	GCM All Cell Average	GCM Upper Cell
Simulated 6ka Sediment (T/month)	247862.9	386795.2	6528728.4	209866.2	402153.5	507897.8
Control 0ka Sediment (T/month)	2019542.3	3013809.0	3557785.9	108599.8	182967.0	409430.9
6ka Sed0ka_SedJ	0.2	0.3	0.8	0.9	1.2	0.2
%difference	22.7	28.3	83.5	93.2	119.8	24.0
6ka-0ka	459020.6	853986.2	2970942.5	101256.3	219186.4	98466.8
	6ka GCM4		6ka GCM2		6ka GCM5	
	GCM All Cell Average	GCM Upper Cell	GCM All Cell Average	GCM Upper Cell	GCM All Cell Average	GCM Upper Cell
Simulated 6ka Sediment (T/month)	4717209.2	857128.8	17516838.0	711826.3	989572.7	944349.0
Control 0ka Sediment (T/month)	2019542.3	3013809.0	3557785.9	108599.8	182967.0	409430.9
ratio	1.3	1.8	3.9	5.6	4.4	1.3
%difference	133.6	182.6	392.4	555.5	440.8	130.6
6ka-0ka	2697867.0	5503319.8	13959052.1	603226.4	806605.6	534918.0
	6ka GCM4		6ka GCM2		6ka GCM5	
	GCM All Cell Average	GCM Upper Cell	GCM All Cell Average	GCM Upper Cell	GCM All Cell Average	GCM Upper Cell
Simulated 6ka Sediment (T/month)	1077292.3	1275457.6	1395192.0	24505.3	113185.0	234185.6
Control 0ka Sediment (T/month)	2019542.3	3013809.0	3557785.9	108599.8	182967.0	409430.9
ratio	-0.5	-0.6	-0.6	-0.8	-0.4	-0.4
%difference	-46.7	-57.7	-60.8	-77.4	-38.1	-42.8
6ka-0ka	-942250.0	-1738351.4	-2162593.9	-84094.5	-69782.0	-175245.4
	6ka GCM4		6ka GCM2		6ka GCM5	
	GCM All Cell Average	GCM Upper Cell	GCM All Cell Average	GCM Upper Cell	GCM All Cell Average	GCM Upper Cell
Simulated 6ka Sediment (T/month)	247862.9	386795.2	6528728.4	209866.2	402153.5	507897.8
Control 0ka Sediment (T/month)	2019542.3	3013809.0	3557785.9	108599.8	182967.0	409430.9
6ka Sed0ka_SedJ	0.2	0.3	0.8	0.9	1.2	0.2
%difference	22.7	28.3	83.5	93.2	119.8	24.0
6ka-0ka	459020.6	853986.2	2970942.5	101256.3	219186.4	98466.8
	6ka GCM4		6ka GCM2		6ka GCM5	
	GCM All Cell Average	GCM Upper Cell	GCM All Cell Average	GCM Upper Cell	GCM All Cell Average	GCM Upper Cell
Simulated 6ka Sediment (T/month)	4717209.2	857128.8	17516838.0	711826.3	989572.7	944349.0
Control 0ka Sediment (T/month)	2019542.3	3013809.0	3557785.9	108599.8	182967.0	409430.9
ratio	1.3	1.8	3.9	5.6	4.4	1.3
%difference	133.6	182.6	392.4	555.5	440.8	130.6
6ka-0ka	2697867.0	5503319.8	13959052.1	603226.4	806605.6	534918.0
	6ka GCM4		6ka GCM2		6ka GCM5	
	GCM All Cell Average	GCM Upper Cell	GCM All Cell Average	GCM Upper Cell	GCM All Cell Average	GCM Upper Cell
Simulated 6ka Sediment (T/month)	1077292.3	1275457.6	1395192.0	24505.3	113185.0	234185.6
Control 0ka Sediment (T/month)	2019542.3	3013809.0	3557785.9	108599.8	182967.0	409430.9
ratio	-0.5	-0.6	-0.6	-0.8	-0.4	-0.4
%difference	-46.7	-57.7	-60.8	-77.4	-38.1	-42.8
6ka-0ka	-942250.0	-1738351.4	-2162593.9	-84094.5	-69782.0	-175245.4

DISCUSSION

Monsoon strength and impacts on sediment through time

Slight changes in the boundary conditions between 0 ka BP and 6 ka BP facilitate simple postulation about monsoonal forcing. Based on pre-industrial green-house gas values, the 0 ka BP models reasonably represent the present-day climate in the Rio Grande watershed. Inputs for the 6 ka BP model remain nearly the same as the 0 ka BP control run, except for the solar insolation values (and slight changes in greenhouse gases), which lead to more intense solar radiation during summer months and weakened solar insolation during winter months. Though the summertime insolation was a maximum at approximately 11 ka BP, the summer solar radiation received and modeled for 6 ka BP is still much higher than today. As the monsoon is forced by differing temperatures on the sea and land surface, it is reasonable to expect the summertime monsoon to be even stronger at 9 ka than 6 ka BP; which may bring more precipitation and provide more sediment from the Rio Grande to the GOM. However, this study shows that increased monsoonal precipitation is not the only way by which the NAM can force higher sedimentation rates.

Higher monsoonal intensity is plausible with greater energy input into the system with higher solar insolation, but that may not necessarily imply greater precipitation with similar storm styles. It is plausible that monthly precipitation remained the same or even decreased, but storm intensity dramatically increased. As shown in figure 17, increased storm intensity more greatly affects sediment flux than constant storm intensity with increased precipitation values. Though this mechanism of monsoonal forcing on sediment flux through the system is reasonable, it is more difficult to test, given such coarse model resolution.

Volumetric evidence suggests there are more questions to be answered than the first-order scope of this project may allow. The dimensions for Banfield's TST 1B (11.5 ka), TST 2B (9.5 ka), and TST 4 (5.6 ka) are respectively 50km x 30km x 22.5m, 30km x 25km x 15m, and 85km x 70 km x 24.5m, and corresponding volumes are respectively: 33.8, 11.3, and 145.7 km³ (Banfield, 1998). The proposed simple model discussed in the previous paragraph justifies maximum sediment flux at 9 ka, however a relative minimum sediment volume is interpreted from the seismic survey. Although this study suggests a stronger monsoon and more sediment flux for that time, climate is not the only forcing mechanism for sediment deposition into the Gulf. Banfield (1998) identified onlapping fill reflections in the seismic record that suggests that TST 4 is comprised of gravity flow deposits, driven by low-velocity turbidity currents. Suspended sediment is the primary source of sediment in a low density flow, but the means of suspension and flow density could vary (Lowe, 1982). Therefore the amount of deposition may or may not indicate sediment flux in the onshore fluvial system.

Sediment Simulation Method

As described earlier, the method used to simulate the sediment flux for a given month is based on a single basin-wide storm event. The stream discharge values outputted from that simulation were then multiplied by the number of storms per month before being entered into the sediment rating curve. If basin-wide storms did occur multiple times per month in this fashion, subsequently greater flow than the resultant flow values observed earlier would be observed. Because of the time required for all the storm water to reach the river and run off, the storms would feedback into each other, creating subsequently greater discharge values. For this reason,

the method presented in this paper gives a low-end estimate of sensitivity of the watershed to changes in precipitation.

The Younger Dryas

The 11.5 ka transgressive event could also be explained by the Younger Dryas. The Younger Dryas is a cooling event that occurred 12,900 to 11,500 years ago. The cause is debated, but multiple theories exist. For example, Broecker (2006) proposed that the thermohaline circulation pattern was disrupted by a freshwater flood of glacial Lake Agassiz into the Atlantic Ocean. Another theory is that the jet stream shifted northward as a result of the receding ice sheet, which brought excess rain into the North Atlantic and disrupted the thermohaline circulation pattern (Eisenman et al., 2009). Though the cause of the Younger Dryas is not completely known, it did have a cooling effect on North America. Even with precipitation held constant, cooler climate would increase effective precipitation by decreasing evaporation (Hodge et al., 2008) and allow more water to reach streams. Alternately, the general cooling of the northern hemisphere is thought to have reversed oceanic transgression or, at least, stalled sea-level rise (McCulloch et al., 1999). With sedimentation held constant during a sea-level stall or fall, the Rio Grande delta would respectively prograde or aggrade (increased turbidite potential) from the position at that time. Though a strong monsoon effect could be a reasonable explanation for higher sediment yield for 11.5 ka, it can readily be explained by the Younger Dryas. This pause in sea level is far less likely an explanation for TST 2 and 4.

Model simplicity and bedload

The models and simulations used for this study are designed only to be of first order evaluation. This test of possible monsoon influence is not intended to model sediment flux in its

entirety, nor is it intended to accurately estimate current sediment flux. Tests used within this study are designed to understand hypothetical changes. The empirical sediment data used for this study are all suspended sediment samples. This does not include bedload, but it was established that most rivers carry about 10% of their sediment as bedload (Csermak and Rakoczi, 1987). Bedload values also tend to vary based on the sediment material making up the bed and the concentration of suspended load. For sand-based rivers, suspended sediment concentrations less than 1000 ppm relate to bedloads of 25-150% of the suspended load; while suspended concentrations over 7500 ppm will have related bedloads of 5-15% of the suspended load. Gravel, rock, or consolidated clay-based rivers with suspended sediment concentrations of less than 1000 ppm or more than 7500 ppm vary from 5-12% to 2-8%, respectively, based on the same concentrations (Morisawa, 1985; Lane and Borland, 1951).

Future work

Though this study shows that monsoonal influence is a plausible forcing mechanism for increased sediment deposition, there are other questions that may need to be answered, such as those regarding storm intensities and change in curve number over time. Closer looks at existing GCM results or new GCM simulations may reveal that storm intensities were significantly different from 5.5 to 11.5 ka BP. If the intensities were higher, that would reasonably explain storm intensity as a forcing mechanism for prograding deltaic deposition. Work to understand infiltration and runoff within a different climate also needs to be completed to more accurately simulate this watershed. For example, proxy data suggest average climate was drier from 5-10 ka BP. This drier climate would dictate vegetation type and soil cohesion. Such changes would greatly affect runoff, erosion, and sediment flux.

Results from the 6 ka BP precipitation anomaly analysis show heightened spring precipitation. If this precipitation is received as rain water, it would no doubt affect sediment flux within the river system. Because this study was focused on testing the sensitivity of sediment flux to NAM effects, patterns and mechanisms of this heightened spring precipitation were not investigated. These simulation results suggest that the NAM is one of many factors possibly affecting sediment flux within the Rio Grande River watershed.

CONCLUSION

Given this simple look at monsoonal precipitation and its potential impact on suspended sediment flux through the New Mexico portion of the Rio Grande, the following can be concluded:

1. Large pulses of sediment reaching the GOM during the early to middle Holocene can be driven by monsoonal forcing. Though this study did not attempt to reconcile all modern influences on the watershed system, it did show that suspended sediment transport could have been increased by 79% during times of heavy monsoonal rainfall six thousand years ago.

Increased precipitation is not the only mechanism by which sediment flux can be increased.

2. Increases in average monsoonal precipitation can increase the flux of sediment through the system. This study also showed that how the precipitation was received can have an even bigger influence on sediment flux through the system. As illustrated in figure 17, even a decrease in monthly monsoonal precipitation can increase sediment flux if the storms are more intense. Decrease in storm frequency and increase in storm intensity appear to be more effective in promoting sediment flux through the Rio Grande.

3. Both conclusions 1 and 2 can be used to explain increased sediment flux in the system. Modeled changes of both storm intensity and average monthly precipitation are effective on sediment flux, but individual effects are not enough to explain the mechanisms by which sediment did increase. A combination of increased monthly monsoonal precipitation **and** increased storm intensity is more likely to have effectively increased sediment flux.

REFERENCES

- Adams, D.K. and Comrie, A.C., 1997, The North American monsoon, *Bulletin of the American Meteorological Society*, v. 78 (10), p. 2197-2213
- Adsero, C.M., 2008, NRCS curve number calibration using USGS regression equations, Master's Thesis, Civil Engineering, Brigham Young University.
- Amin, I.E. and Jacobs, A.M., 2007, Accounting for sediment sources and sinks in the linear regression analysis of the suspended sediment load of streams: The Rio Puerco, New Mexico, as an example; *Environmental Geosciences*, v. 14, p. 1-14
- Applegarth, J. S., 1979, Herpetofauna (anurans and lizards) of Eddy County, New Mexico: Quaternary changes and environmental implications. Ph.D. Dissertation, University of New Mexico, Albuquerque, 258 pp
- Atkinson, E.L., 2001, Natural Resources conservation service curve number analysis for Texas, Master's Thesis, Civil Engineering, Texas Tech.
- Balsillie, J.H. and Donoghue, J.F., 2004, High resolution sea-level history for the Gulf of Mexico since the last glacial maximum, *Florida Geological Survey Report of Investigations 103*, pp. 66
- Banfield, L., and Anderson, J.B., 2004, "The Late Quaternary Evolution of the Rio Grande Delta." *Special Publication, Society of Sedimentary Research*, v. 79, p. 289-306
- Banfield, L., 1998, Quaternary evolution of the Rio Grande Delta, PhD, Doctoral, Rice University, pp. 232
- Bard, E., B. Hamelin, M. Arnold, L. Montaggioni, G. Cabioch, and G. Faure, 1996, Deglacial sea-level record from Tahiti corals and the timing of global meltwater discharge: *Nature*, v. 382, p. 241-244

- Berger, A.L., 1992, Orbital Variations and Insolation Database, IGBP PAGES/World Data Center for Paleoclimatology, Data Contribution Series # 92-007, NOAA/NGDC Paleoclimatology Program, Boulder CO, USA
- Berger, A.L., 1978, Long-term variations of caloric insolation resulting from the earth's orbital elements, *Quaternary Research*, v. 9, p. 139-167
- Berryhill, H. L., Jr., G. L. Shideler, C. W. Holmes, G. W. Hill, S. S. Barnes, and R. G. Martin, Jr., 1976, *Environmental Studies, South Texas Outer Continental Shelf*, Reston, V A, United States Geological Survey.
- Blum, M.D. and Tornqvist, T.E., 2000, Fluvial responses to climate and sea-level change: a review and look forward. *Sedimentology*, v. 47 (Supplement): p. 2-48
- Braconnot, P., Otto-Bliesner, B., Harrison, S., Joussaume, S., Peterschmitt, J.Y., Abe-Ouchi, A., Crucifix, M., Driesschaert, E., Fichefet., Th., Hewitt, C.D., Kageyama, M., Kitoh, A., Lâiné, A., Loutre, M.F., Marti, O., Merkel, U., Ramstein, G., Valdes, P., Weber, S.L., Yu, Y., Zhao, Y., 2007, Results of PMIP2 coupled simulations of the Mid-Holocene and Last Glacial Maximum – Part 1: experiments and large-scale features, *Climate of the Past*, v., 3 (2), p. 261-277
- Broecker, W.S., 2006, Was the Younger Dryas triggered by a flood?, *Science*, v. 312, p 1146-1148.
- Brook, G.A., Ellwood, B.B., Railsback, L.B., and Cowart, J.B., 2006, A 164 ka record of environmental change in the American Southwest from a Carlsbad Cavern speleothem, *Palaeogeography, Palaeoclimatology, Palaeoecology*, v., 237, p. 483-507
- Bryson, R. and Lowry, W.P., 1955, Synoptic climatology of the Arizona summer precipitation singularity, *Bulletin of the American Meteorological Society*, v. 36, p. 329-339

- Buck, B.J. and Monger, C., 1999, Stable isotopes and soil-geomorphology as indicators of Holocene climate change, northern Chihuahuan Desert, *Journal of Arid Environments*, v. 43, p. 357-373
- Coats, L.L., Cole, K.L., and Mead, J.I., 2008, 50,000 years of vegetation and climate history on the Colorado Plateau, Utah and Arizona, USA, *Quaternary Research*, v. 70 (2), p. 322-338
- Csermak, B. and Rakoczi, L., 1987, Erosion and sedimentation, *In* Starosolszky, O. (ed) *Applied Surface Hydrology*, pp. 760-807, Water Resource Publications, Littleton, CO
- Curry, J.R., 1959, Sediments and History of Holocene transgression, continental shelf, Northwest GOM, dissertation, University of California, Scripps Institution of Oceanography, pp. 46.
- Davis, O.K. and Shafer, D.S., 1992, A Holocene climatic record for the Sonoran Desert from pollen analysis of Montezuma Well, Arizona, USA, *Paleogeography, Paleoclimatology, Paleoecology*, v., 92, p. 107-119
- Douglas et al, 1993, The Mexican monsoon, *Journal of Climate*, v. 6, p. 1665-1667
- Eisenman, I., Bitz, C.M., Tziperman, E., 2009, Rain driven by receding ice sheet as a cause of past climate change., *Paleoceanography*, v. 24, PA4209, doi:10.1029/2009PA001778.
- Gordon, N.D., McMahon, T.A., Finlayson, B.L., Gippel, C.J., and Nathan, R.J., 2004, *Stream Hydrology: An introduction for Ecologists*, 2E, John Wiley & Sons, Ltd., West Sussex, pp. 429
- Graf, W. L., 1994, *Plutonium and the Rio Grande: Environmental Change and Contamination in the Nuclear Age*: New York, Oxford University Press, Inc. 329 p. Poore et al (2005)

- Harrington, J.A., Jr., Cervený, R., and Balling Jr., R., 1992, Impact of the Southern Oscillation on the North American Southwest Monsoon, *Physical Geography*, v. 13, p. 318-330.
- (HEC) Hydrologic Engineering Center, 1998, HEC-1 Flood Hydrograph Package User's Manual, US Army Corp of Engineers
- Hodge, E.J., Richards, D.A., Smart, P.L., Andreo, B., Hoffmann, D.L., Matthey, D.P., and Gonzalez-Ramon, A., 2008, Effective precipitation in southern Spain (~266 to 46 ka) based on a speleothem stable carbon isotope record, *Quaternary Research*, v. 69, p. 447-457.
- Holliday, V.T., 1989, Middle Holocene Drought on the Southern High Plains, *Quaternary Research*, v. 31, p. 74-82.
- Holmgren, C.A., Betancourt, J.L., and Rylander, K.A., 2006, A 36,000-yr vegetation history from the Peloncillo Mountains, southeastern Arizona, USA, *Palaeogeography, Palaeoclimatology, Palaeoecology*, v. 240, p. 405-422
- Hjulstrom, F., 1939, Transportation of detritus by moving water: Part 1 Transportation *in* Recent Marine Sediments, AAPG Special Volumes 10
- Kiehl, J. T. and Trenberth, K.E., 1997, Earth's Annual Global Mean Energy Budget, *Bulletin of the American Meteorological Society*, v. 78 (2)p.197–208
- Knighton, D., 1984, *Fluvial Forms and Processes*, Edward Arnold, London
- Lambeck, K. and Chappell, J., 2001, Sea level change through the last glacial cycle, *Science*, v. 292, p. 679-686
- Lane, E.W. and Borland, W.M., 1951, Estimating bedload, *American Geophysical Union Transactions*, v. 32, p. 121-123 (as cited by Gordon et al, 2004)

- Leopold, L.B., and Maddock, T., 1953, The hydraulic geometry of stream channels and some physiographic implications, USGS Professional Paper 252, pp. 57
- Levings, G.W., Healy, D.F., Richley, S.F., and Carter, L.F., 1998, Water Quality in the Rio Grande Valley, Colorado, New Mexico, and Texas, 1992-1995, U.S., Geological Survey Circular, v. 1162, pp. 39.
- Lowe., D.R., 1982, Sediment gravity flows: II depositional models with special reference to the deposits of high-density turbidity currents, *Journal of Sedimentary Petrology*, v. 52, p. 279-297
- Mack, G.H., Seager, W.R., Leeder, M.R., Perez-Arlucea, M., and Salyards, S.L., 2006, Pliocene and Quaternary history of the Rio Grande, the axial river of the southern Rio Grande rift, New Mexico, USA, *Earth Science Reviews*, v. 79 (1-2), p. 141-162.
- Berryhill, H. L., Jr., G. L. Shideler, C. W. Holmes, G. W. Hill, S. S. Barnes, and R. G. Martin, Jr., 1976, *Environmental Studies, South Texas Outer Continental Shelf*, Reston, V A, United States Geological Survey.
- Manz, L.R., Sarkar, D., and Hammond Jr., W.W., 2005, Water resources and water quality in the Rio Grande Valley of Texas: Current status and future projections, *Environmental Geosciences*, v. 12 (3), p. 193-206.
- McCulloch, M.T., Tudhope, A.W., Esat, T.M., Mortimer, G.E., Chappell, J., Pillans, B., Chivas, A.R., and Omura, A., 1999, Coral record of equatorial sea-surface temperatures during the penultimate deglaciation at Huon Peninsula, *Science*, v. 283, p. 202–204
- McMillan, M.E., Heller, P.L., Wing, S.L., 2006, History and causes of post-Laramide relief in the Rocky Mountain orogenic plateau, *GSA Bulletin*, v. 118 (3/4), p. 393-405
- Goldstein and Harrison, 1999

- Morisawa, M.E., 1985, *Rivers, Form and Process, Geomorphology Texts 7*, Longman, London
(as cited by Gordon et al, 2004)
- National Atlas of the United States, 2006, Major Dams of the United States, available online 8 April 2010, <http://nationalatlas.gov/mld/dams00x.html>
- NODC, 1998, National Oceanographic Data Center, NOAA, Washington, D.C.
- Peltier, W.R., 2004, Global glacial isostasy and the surface of the ice-age Earth: the ICE-5G (VM2) model and GRACE. *Annual Review of Earth and Planetary Sciences*, v. 32, p. 111-149
- Poore, .R.Z., Pavich, M.J., and Grissino-Mayer, H.D., 2005, Record of the North American southwest monsoon from Gulf of Mexico sediment cores, *Geology*, v. 33, p. 209-212.
- Price, C.V., Nakagaki, N., Hitt, R.M., 2007, Enhanced Historical Land-use and Land-Cover Data Sets of the U.S. Geological Survey: polygon format files, 1E, USGS, http://water.usgs.gov/lookup/getspatial?ds240_landuse_poly.
- PRISM Climate Group, Oregon State University, <http://www.prismclimate.org>, created 4 Feb 2004
- Reitan, C.H., 1957, The role of precipitable water vapor in Arizona's summer rains. Tech. Rep. on the Meteorology and Climatology of Arid Regions 2, Institute of Atmospheric Physics, University of Arizona, Tuscon, 19 pp.
- Ruddiman, W.F., 2008, *Earth's Climate, Past and Future, 2E.*, W. H. Freeman and Company, USA, pp. 388
- Rupper, S. and Koppes, M., 2010, Spatial patterns in Central Asian climate and equilibrium line altitudes, *IOP Conference Series: Earth and Environment Science*, v., 9 (1), p. 1-7

- Rupper, S., Roe, G., and Gillespie, A., Spatial patterns of Holocene glacier advance and retreat in Central Asia, *Quaternary Research*, v. 72 (3), p. 331-346
- Schmitt, C.J., Dethloff, G.M., Hinck, J.E., Bartish, T.M., Blazer, V.S., Coyle, J.J., Denslow, N.D., Tillitt, D.E., 2004, Biomonitoring of environmental status and trends (BEST) program: Environmental contaminants and their effects on fish in the Rio Grande basin, United States Geological Survey, Scientific Investigations Report 2004-5108, 118 pp
- Schmitz, T.J., and Mullen, S.L., 1996, Water vapor transport associated with the summertime North American monsoons as depicted by ECMWF analyses, *Journal of Climate*, v. 9, p. 1621-1633.
- Schumm, S.A., 1993, River Response to Baselevel Change: implications for Sequence Stratigraphy, *Geology*, v. 101 (2), p. 279-294
- Soil Survey Staff, Natural Resources Conservation Service, United States Department of Agriculture. U.S. General Soil Map (STATSGO2). Available online at 'http://soildatamart.nrcs.usda.gov accessed 01/12/2010'.
- Syvitski, J.P.M. and Andrews J.T., 1994, Climate change: Numerical modeling of sedimentation and coastal processes, *Eastern Canadian Arctic, Arctic and Alpine Research*, v. 26, p. 199-212
- Van Wagoner, J.C., Mitchum, R.M., Campion, K.M., and Rahmanian, V.D., 1990, *Siliciclastic Sequence Stratigraphy in Well Logs, Cores, and Outcrops*, American Association of Petroleum Geologists, Tulsa, 55 p.

- Wallace, S.B., McGee, D., Adams, K.D., Cheng, H., Edwards, R.L., Oviatt, C.G., and Quade, J., 2009, A Great Basin-wide dry episode during the first half of the Mystery Interval?, *Quaternary Science Reviews*, v. 28, p. 2557-2563
- Watson, A.W., Holle, R., and Lopez, R.E., 1994, Diurnal cloud-to-ground lightning and upper-air patterns in Arizona during the southwest monsoon, *Mon. Wea. Rev.*, v. 122, 1716-1725.
- Wellner, J.S., Fraticelli, C.M., Anderson, J.B., and Banfield, L.A., 2000; Efficacy of climate variations on sediment yield: a comparison of the Brazos/Colorado, western Louisiana, and Rio Grande Fluvial systems during the last glacial-eustatic cycle; *Gulf Coast Association of Geological Societies Transactions*, v. 50, p. 679-686
- Wellner, R., and Bartek, L.R., (2003), The Link Between Base-level, Climate, Shelf Physiography and Large Incised Valley Development: A Modern Example from the East China Sea, *Journal of Sedimentary Research*, v. 71, No. p. 926-940.
- Weng, C., and Jackson, S.T., 1999, Late glacial and Holocene vegetation history and paleoclimate of the Kaibab Plateau, Arizona, *Paleogeography, Paleoclimatology, Paleoecology*, v. 153, p.179-201
- Wilkins, D.E. and Currey, D.R., 1999, Radiocarbon chronology and ^{13}C analysis of mid-to late-Holocene aeolian environments, Guadalupe Mountains National Park, Texas, USA, *The Holocene*, v. 9, p. 363-371
- USDA, 1986, Urban Hydrology for Small Watershes, NRCS CED Technical Release 55.
- USGS, 2003, A Tapestry of Time and Terrain: The union of two maps - geology and topography, Online

Zhua, Y-M, Lua, X.X., and Zhou Y., 2008, Sediment flux sensitivity to climate change: A case study in the Longchuanjiang catchment of the upper Yangtze River, China, *Global and Planetary Sciences*, v. 60 (3-4), p. 429-442